PAPER: Classical statistical mechanics, equilibrium and non-equilibrium

Tracer dynamics in one dimensional gases of active or passive particles

Tirthankar Banerjee[1,*]**, Robert L Jack**[1,2] **and Michael E Cates**[1]

[1] DAMTP, Centre for Mathematical Sciences, University of Cambridge, Wilberforce Road, Cambridge CB3 0WA, United Kingdom
[2] Yusuf Hamied Department of Chemistry, University of Cambridge, Lensfield Road, Cambridge CB2 1EW, United Kingdom
E-mail: tb698@cam.ac.uk

Abstract. We consider one-dimensional systems comprising either active run-and-tumble particles (RTPs) or passive Brownian random walkers. These particles are either noninteracting or have hardcore exclusions. We study the dynamics of a single tracer particle embedded in such a system—this tracer may be either active or passive, with hardcore exclusion from environmental particles. In an active hardcore environment, both active and passive tracers show long-time sub-diffusion: displacements scale as $t^{1/4}$ with a density-dependent prefactor that is independent of tracer type, and differs from the corresponding result for passive-in-passive subdiffusion. In an environment of noninteracting active particles, the passive-in-passive results are recovered at low densities for both active and passive tracers, but transient caging effects slow the tracer motion at higher densities, delaying the onset of any $t^{1/4}$ regime. For an active tracer in a passive environment, we find more complex outcomes, which depend on details of the dynamical discretization scheme. We interpret these results by studying the density distribution of environmental particles around the tracer. In particular, sticking of environment particles to the tracer cause it to move more slowly in noninteracting than in interacting active environments, while the anomalous behaviour of

*Author to whom any correspondence should be addressed.

the active-in-passive cases stems from a 'snowplough' effect whereby a large pile of diffusive environmental particles accumulates in front of an RTP tracer during a ballistic run.

Keywords: active matter, Brownian motion, exclusion processes, persistence

Contents

1. Introduction

The problem of a tagged particle in single-file diffusion has been of interest to physicists for more than five decades [1–6], since its inception in the study of transport through ion channels in cell membranes [7]. Applications include colloidal motion [8]; motion in super-ionic conductors [2]; protein translocation along DNA [9]; diffusion in zeolites [10]; and interacting Markov chains [11]. The properties of a tagged particle reveal important features about the environment it is embedded in. Single file motion takes place when particles move through such narrow channels that no overtaking is allowed, and also in cases where nano-scale objects move along one-dimensional (1D) filaments [12]; the initial order of particles is thereby maintained in single file motion. This leads to the emergence of long-time correlations in the system, which means that the mean squared displacement of the tagged particle grows for large time as $\sqrt{t}$, in contrast to the linear scaling for freely diffusing particles [4, 8]. However, this subdiffusive displacement still follows a Gaussian distribution [8]. Heuristically, one can explain this scaling by saying that at time t, the number n of particles in diffusive contact scales as $\sqrt{t}$, while the single-file rule enslaves all the particles to their centre of mass, whose diffusivity is reduced by a factor of n from that of a free particle; thus $\mathrm{d}\langle r^2\rangle/\mathrm{d}t \sim t^{-1/2}$. Tagged particle studies have also appeared in problems related to biased one dimensional systems such as asymmetric exclusion process [13] or random average processes [14].

Properties of non-interacting *active* particles, such as run-and-tumble particles (RTPs) [15–17], typically become indistinguishable from those of non-interacting passive Brownian particles at long times, for suitably chosen parameters [18]. A free RTP runs ballistically at speed v in a certain direction, tumbles and chooses a new random direction for the next run; this motion approximates that of *E. coli* bacteria [15]. This leads to temporal correlations in the particle velocity, with a range of the order of the flip time γ^{-1} [18]. This finite persistence time leads to several interesting features. For example, at the single-particle level one finds non-Boltzmann steady states in confining potentials [19, 20], first order dynamical transitions [21], and as recently shown in [22]—in d dimensions, a *condensation* transition (between a fluid phase and a condensed phase) where the order of the transition itself can be tuned upon varying d and a given velocity distribution. The behaviour of RTPs in disordered potentials [23] and with stochastic resetting [24] have also been studied. Collective motion has been studied at the level of two interacting RTPs [25–28] and, in more phenomenological terms, for the full many-body problem where hard-core exclusion leads to motility-induced phase separation (MIPS) [29].

The problem of tagged active particles in crowded environments has also been extensively studied; see [30] for a review. Some important works in this context include RTPs interacting via harmonic forces in 1D [31, 32], and exclusion in 2D [31]; a tagged RTP embedded in a system of passive particles executing symmetric exclusion process [33]; and discrete lattice models for bacterial motion [34, 35]. Distribution functions of tagged particle positions have also been calculated for systems with smooth potentials [36].

In the context of active particles, a hardcore tracer is somewhat like a mobile boundary wall, in the sense that the environmental particles cannot cross it. While the pressure

Table 1. Table summarizing alphabetic system codes used in the text. There are eight possible cases, all of which we discuss.

Code	Environment	Tracer	Interaction
PPH [4–6]	Passive	Passive	Hardcore
PAH [33, 41, 42]	Passive	Active	Hardcore
AAH [31, 35, 39]	Active	Active	Hardcore
APH [41–45]	Active	Passive	Hardcore
PPN [5, 6, 48]	Passive	Passive	Non-interacting
AAN	Active	Active	Non-interacting
APN [41–47]	Active	Passive	Non-interacting
PAN [41, 42]	Passive	Active	Non-interacting

exerted on confining walls has been studied [37, 38], the question of how hardcore passive and active tracers behave in a sea of RTPs still remains open. That is the question that we address here.

To fix nomenclature, we refer to a single *tracer particle* in a sea of *environmental particles*. We identify eight separate problems (see table 1), depending on whether the environmental particles are hardcore or noninteracting, whether they are active (RTP) or passive (Brownian), and whether the hardcore tracer is itself active or passive. Several of these cases have been studied before, but to the best of our knowledge, they are yet to be systematically compared under a common umbrella. This is the main goal of the current paper. To make the comparisons manageable we always choose the long-time free diffusivities of active and passive particles to be equal, and start from an equispaced initial condition of a large (but finite) packet of particles, in an unbounded domain, with the tagged particle at the centre. All particles are *pointlike*, so the most important control parameter is initial density of the environmental particles, nondimensionalized by the RTP run length v/γ. If all particles are passive then the run length has no meaning, and the density merely rescales the time variable; see section 3 below.

We use numerical simulations to analyse and compare the eight problems shown in table 1, which we identify by a three-letter short-hand code whose first letter refers to the environment particles as active (RTPs, A) or passive (Brownian walkers, P); the second letter does the same for the tracer; and the third labels whether the environment particles are mutually non-interacting (N) or hardcore (H). We will use lowercase x as a wildcard character when discussing more than one case at a time (e.g. *xxN* means all four cases with a noninteracting environment).

Table 1 cites prior literature arising in various different contexts, some close to the present one and some not. For instance *PPH* has been a cornerstone for tagged particle studies like ours [4–6], whereas *AAH* has been studied in two dimensions [31], with periodic boundaries [35], or with pre-set maximum occupancy per lattice site [39]. Tracer motion in the context of RTPs under single-file constraint with a finite interaction-range was recently studied in [40]. The *PAH* case has been investigated on a lattice in one dimension [33]. Cases *APH*, *APN*, *PAN*, like *PAH*, all involve mixtures of active and passive particles; these are well studied in terms of phase separation

[41, 42] but not single-file diffusion. Similarly APH and APN belong to the large family of problems on passive probes in active media, see, e.g. [43–45]. For non-interacting RTPs and Brownian particles there is of course a huge literature; however there are relatively few studies on hardcore tracers in these systems (cases AAN and PPN). Note also that for tracer diffusion, PPN is identical to PPH for reasons given in section 3 below [5, 6, 48, 49].

Among the main results of our work are the following: (i) in hardcore active environments for both active (AAH) and passive (APH) tracers, the typical displacement scales as $t^{1/4}$ at late times, with a prefactor that scales differently with density from the known PPH case [4]; (ii) in non-interacting but dense active environments (AxN), the typical displacement of a tracer shows deviations from the $t^{1/4}$ scaling law for both passive and active tracers for all times we can access (figure 12); (iii) an active tracer in a passive environment (PAx) can have a much larger long-time typical displacement than in the corresponding active medium (AAx); (iv) in an active environment, adding hardcore interactions to the environment particles (AxH) can *increase* the motion of the tracer compared to the noninteracting counterpart (AxN). We connect many of these results with nontrivial evolutions of the density profile of particles in the medium around the tracer position, including the sticking of particles to the tracer (in active noninteracting environments, AxN) and, separately, the 'snowploughing' of particles by an active tracer (in passive environments, PAx).

The rest of the article is organised as follows: in section 2 we introduce the different interacting models, the numerical schemes used to study them, and the observables. Section 3 recapitulates known results for the two all-passive cases (PPx). Results for AxH, along with a comparison with PPH are presented in section 4.1. Then we study the corresponding non-interacting baths with both passive and active tracers (AxN), and compare with PPN, in section 4.2. We present our results for an active tracer in passive environments (PAx) separately in section 5. After a discussion in section 6 we summarize in section 7. Appendices addressing some technical aspects follow thereafter.

2. Numerical strategy and observables

For each case in table 1 we investigate the statistics of the position of the tracer. In all our studies, the tracer is the central one among $N + 1$ point particles residing initially in a packet spanning $\pm L$ on the infinite line (with the tracer at the origin, $x = 0$). The initial condition is fixed (quenched) with all particles equispaced at time $t = 0$ [4, 18, 50]. The terminology of annealed and quenched initial conditions is borrowed from studies on disordered systems, as a mathematical correspondence exists in averaging over fluctuating (*annealed*) or fixed (*quenched*) initial configurations/disorder distributions [50]; indeed long-time results for 1D Brownian systems are known to be sensitive to the choice of initial conditions [4, 18, 50, 51]. A schematic of the set-up is shown in figure 1. The initial density $\rho = N/(2L)$ is a parameter of the model. For large N the overall density around the tracer does not evolve much on the time scale of our simulations, but finite-size effects due to the packet spreading are detectable in some cases. We discuss these as they arise.
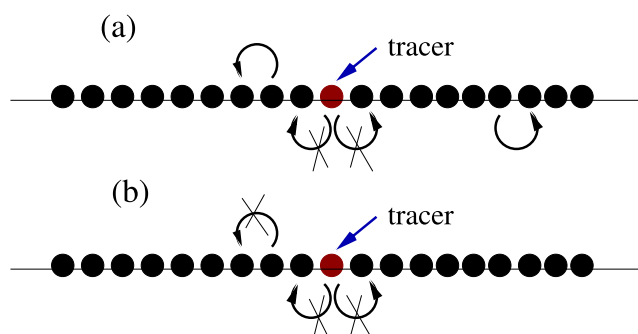
Figure 1. Schematic representation of the initial configurations for: (a) non-interacting and (b) hardcore environments. The environment (black particles) as well as the tracer (central red particle) can be either passive or active. The tracer always interacts with its environment through hardcore exclusion. For environments made up of hardcore particles, the initial ordering of particles is maintained forever. In non-interacting environments, the particles can pass through each other but cannot cross the tracer.

Our systems evolve by a stochastic (Monte Carlo) dynamics with a discrete time step Δt. This might be interpreted as an Euler-type discretization of an underlying continuous-time dynamics, that accounts for the ballistic runs of the RTPs and the hardcore interactions. Alternatively, one may think of active particles whose natural motion involves discrete (finite) steps, so that Δt becomes a parameter of the model itself (as opposed to a numerical time step). These points are discussed further in the later part of this section. Each passive Brownian particle has diffusivity D, and we propose MC updates for their positions by drawing Gaussian-distributed random numbers with zero mean and variance $2D\Delta t$. Each RTP moves with speed v and its orientation is $\tilde{\sigma} = \pm 1$; hence its MC update has proposed displacement of $\tilde{\sigma} v \Delta t$. The orientation changes at a Poisson rate γ [18]. In the initial state, $\tilde{\sigma}$ is assigned randomly ± 1 for each RTP. As noted above, we match the long-time diffusivity of free active and passive particles, which means $D = v^2/(2\gamma)$ [18]. Particle coordinates are updated sequentially in a fixed cyclic sequence $(1 \ldots N + 1)$. This choice is more convenient compared to random sequential updates and in most but not all cases, we find similar results with random sequential updating, see appendix A.

If a proposed MC update does not respect the hardcore interactions of the particles, a collision rule is required. A collision happens if an MC update causes a particle to move beyond one of the neighbours with which it interacts. For systems with hard-core environments (xxH), collisions can take place between any particle i and its neighbours $i \pm 1$ (except that particles $1, N + 1$ each have only one neighbour, of course). For non-interacting environments (xxN) a tracer update may cause a collision with one of its neighbouring environmental particles; an update of environmental particle can lead to a collision with the tracer (but not with another environmental particle).

In all these cases, the collision rule operates as follows: (i) if the collision happens while updating a passive particle, this particle treats its hardcore neighbours as hard walls and reflects off them. Thus the proposed displacement vector for time increment

Δt is folded backward upon reaching a hardcore neighbour until the residual part is short enough to require no further folding. (For a particle with only one hard neighbour, there is at most one fold.) The resultant displacement in Δt does not cross any hardcore neighbour. This scheme is chosen because it respects detailed balance for a system of passive Brownian hardcore particles: if a Monte Carlo move takes a particle from a position say x_s and to say x_e at one time step, then the *reverse* move at any other time step would take the particle from x_e to x_s. Another possible scheme is to interchange particle labels as they meet [5]; also see [52]. (ii) If the collision happens while updating an active particle, there is no detailed balance requirement: the displacement of an RTP is taken (in general) as the minimum of the proposed update and the distance to the nearest hard neighbour in the direction of travel. Hence, when two hardcore RTPs meet head-to-head, the particle being updated stops adjacent to the obstacle particle. Both particles then remain stationary until one or both of them flip(s) direction. If just one particle flips, then both particles subsequently move in this new direction at the same speed. From now on we refer to this as two RTPs *sticking* to each other. Instead, importantly, by a somewhat different mechanism, an RTP can also stick to a passive particle for as long as the attempted displacements of the latter remain smaller than $v\Delta t$. Since these displacements scale as $(D\Delta t)^{1/2}$ the lifetime of such a stuck pair can depend on the discretization time-step. Such dependences influence the tracer dynamics in certain cases, as we elaborate in section 5.1. We note here that our model is tailored to systems where the particles move in discrete (finite) steps in 1D, as happens on actin filaments [12] or microtubules [53]. As a result, Galilean invariance is broken and there is no concept of momentum or force balance: one left-moving particle can arrest the motion of any number of right-movers piled up to its left. Also we address cases where the natural dynamics involves a discrete timestep, associated for instance with the 'walking step' of a myosin motor along an actin filament [12]. Although in many regimes the limit of small timestep is well-behaved and one can think of our model as representing a continuous time process, in some cases the timestep remains relevant even when small. Physically, this corresponds to situations where particles' collective motion retains a dependence on the size of their discrete jumps. In such cases it is important to consider Δt as a parameter of the model, and not as an integration time-step for an underlying continuous process.

To characterise the tracer behaviour, we focus on three observables: (i) the variance of the tracer displacement X as a function of time,

$$\text{Var}(X) = \langle X(t)^2 \rangle - \langle X(t) \rangle^2, \tag{1}$$

which is also its mean squared displacement in symmetric systems where $\langle X \rangle = 0$; (ii) the average density profile $\rho(x, t)$ of particles of the medium; and (iii) the probability distribution $P(X)$ of X for late times $t \gg \gamma^{-1}$.

It is useful to recall how a top-hat initial density $\rho(x, 0)$ spreads in time for free Brownian particles. This is found by solving the diffusion equation for density $\rho(x, t)$ with initial condition

$$\rho(x, 0) = \rho_0 \, ; \quad -L \leqslant x \leqslant L \tag{2}$$
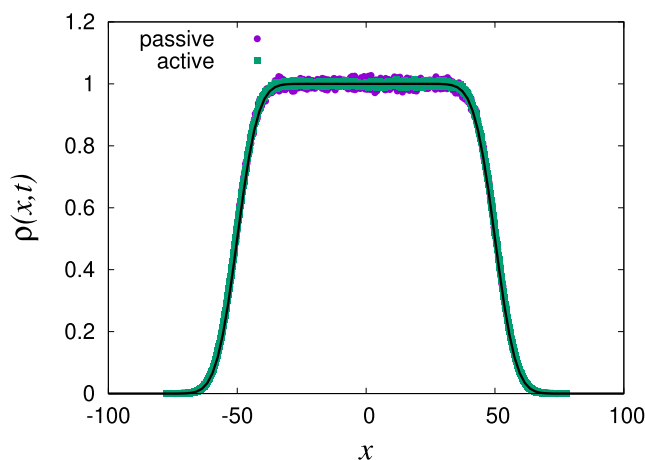
Figure 2. Evolution of a top-hat density profile (equation (2)) for free passive ($D = 0.5$, purple circles) and active ($v = 1 = \gamma$, green squares, green dotted lines) particles obtained at $t = 40 \gg \gamma^{-1}$. Other parameters are $N = 100, L = 50$. Active and passive results coincide. Solid black line represents equation (3). The data for the RTPs has been averaged over 5×10^5 realizations, and that for passive Brownian particles over 1×10^6 realizations.

and $\rho(x, 0) = 0$ otherwise. The solution is

$$\rho(x, t) = \frac{\rho_0}{2} \left[\mathrm{erf}\left(\frac{x + L}{\sqrt{4Dt}} \right) - \mathrm{erf}\left(\frac{x - L}{\sqrt{4Dt}} \right) \right], \tag{3}$$

where $\mathrm{erf}(z) \equiv \frac{2}{\sqrt{\pi}} \int_0^z e^{-y^2} \, \mathrm{d}y$. In figure 2, we compare the behaviour of free RTPs with free Brownian particles, at a late time $t \gg \gamma^{-1}$. (The diffusivities are matched via $D = v^2/2\gamma$, as previously stated.) For both dynamics we have a top-hat initial density on $-50 < x < 50$ with $\rho(x, 0) = 1$, describing $N + 1 = 101$ equispaced particles. The results for the active and passive systems are statistically the same, as expected.

Having specified fully the interactions and discretization strategy, we next study tracer statistics for the various cases enumerated in table 1. We present new results for the active cases in sections 4 and 5 below, but first briefly review and numerically confirm some well-known results for the all-passive cases (PPx), which will serve as a useful benchmark later on.

3. Review of passive tracers in passive environments

3.1. PPH: passive tracer in a hardcore passive environment

The problem of a tagged particle within a system of hardcore Brownian particles has been extensively studied [1–5, 7]. The central result is that the variance $\mathrm{Var}(X)$ of the tracer displacement X scales subdiffusively as $t^{1/2}$. The large-deviation theory for $P(X)$ was developed within the framework of macroscopic fluctuation theory (MFT) in [4], which showed the robustness of the power law, but also the sensitivity of the

prefactor to the choice of initial conditions. Following [4, 49] we have, for a 'quenched' (i.e. equispaced) initial condition of the particles,

$$\text{Var}(X) = \frac{1}{\rho}\sqrt{\frac{2Dt}{\pi}} \equiv \xi_{\text{PPH}}(D, \rho)\sqrt{t}, \tag{4}$$

thereby defining ξ_{PPH} as the 'coefficient of subdiffusion' for case PPH.

It is notable that (4) is obtained in [4] using a general theory for tracer motion in a diffusive fluid environment. The assumptions are those of MFT: on sufficiently long time scales, the collective diffusion of the environment is fully described by two functions which are a diffusivity $D(\rho)$ and a mobility $\sigma(\rho)$. The physical idea is that the tracer motion is slaved to the collective motion of the environment: combined with the hard core constraint, this leads to long-time subdiffusive motion with a coefficient ξ that depends on $D(\rho)$ and $\sigma(\rho)$. For Brownian point particles then $D(\rho) = D$ (the free particle diffusion constant) and $\sigma(\rho) = 2\rho D$, in which case equation (18) of [4] reduces to equation (4) up to a factor of $\sqrt{2}$ that arises due to the quenched initial condition.

Equation (4) holds only at sufficiently late times, because for short times, before meeting another particle, the tracer diffuses freely with $\text{Var}(X) = 2Dt$. By equating this with $\xi_{\text{PPH}}\sqrt{t}$ we identify the crossover time from early to late regimes as

$$t_{\text{cr}} \approx \frac{1}{2\pi\rho^2 D}. \tag{5}$$

Since these are point particles, diffusion has no timescale of its own, and any change in density ρ can be absorbed by rescaling the time unit (at fixed D). This is only true when there is no active particle in the system as holds here for PPx, but not the other six cases in table 1.

To allow later comparisons with these other cases, in figure 3 we plot trajectories for five consecutive hardcore Brownian particles in the middle of a much larger PPH system of $N + 1 = 1001$ particles (with the remaining $N - 4$ trajectories not shown). We also plot $\text{Var}(X)$ for the (central) tracer particle against time, showing the crossover from free diffusion to subdiffusion.

3.2. PPN–PPH correspondence

Case PPN comprises a system of passive point particles in which the tracer particle cannot cross its neighbours but they can cross each other. However, in PPN one can choose to relabel the particles' worldlines as if they had not crossed (but instead had had a hardcore collision) without changing the Brownian trajectories or their statistics in any other way [5, 6, 48, 49]. Therefore, the environment presented to the tracer in case PPN is identical to that for case PPH, so that the tracer statistics are themselves identical at all times. In particular, $\xi_{\text{PPN}} = \xi_{\text{PPH}}$. Put differently, for the two fully passive systems, the only hardcore interaction that matters for tracer dynamics is the one between tracer and environment, which is present in both cases. We also note that this equivalence of world-lines argument for these two fully passive systems is only exact for the continuous time process (i.e. in the limit of $\Delta t \to 0$).
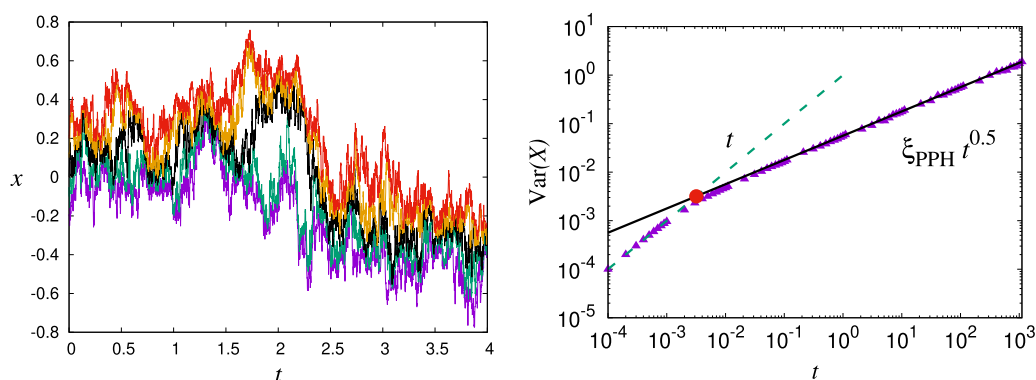
Figure 3. (Left) Trajectories for five consecutive diffusive particles within a much larger ($N = 1000$) *PPH* system. Hardcore exclusion ensures these trajectories never cross each other. (Right) Variance of the tracer position $\text{Var}(X)$ as a function of time t. Solid triangles are the simulation results. The black solid line is equation (4). The red disc marks the typical crossover time t_{cr} from free diffusion to subdiffusion. Parameters are $D = 0.5, N = 2000, \rho = 10, \Delta t = 0.0001$. For $t \leqslant 1$, data averaged over 10^4 realizations; for $t > 1$, data averaged over 900 realizations.

3.3. Finite-size effects

At extremely large times, $Dt \gg L^2$, any finite packet of particles will eventually spread out and reduce in density. Since the non-crossing constraint requires the tracer to occupy the median position among $N + 1$ particles, the tracer position ultimately scales in time like the centre of mass of $n = N$ neighbours. The tracer thus shows free diffusion with diffusivity $\sim D/N$. Hence, there is a second crossover time (dependent on N) beyond which linear time scaling for $\text{Var}(X)$ is restored. In this paper we avoid accessing such timescales as far as possible: we focus on behaviour that is representative of the limit $N, L \to \infty$ (at fixed ρ), so the long-time diffusive regime appears as a finite-size effect (because our simulations have finite N). We mention these finite-size effects when necessary to understand our simulation data, with further discussion in appendix B.

4. Results for active and passive tracers in active environments

In the absence of external forcing or couplings to reservoirs, a collection of passive particles respects local detailed balance; if confined to a finite domain, the system would reach Boltzmann equilibrium. In contrast, if at least one RTP is present, detailed balance is broken. This leads to new phenomena which are absent in the *PPx* cases. Our main goal in the rest of this paper is to elucidate the six cases in table 1 that are not purely passive. We will compare these with the two all-passive cases just reviewed, wherever this is helpful. We first consider hardcore active environments in section 4.1, and subsequently present results for different tracers in non-interacting active media in section 4.2. Then in section 5 we show how the two cases with an active tracer in a passive environment *qualitatively* differ from all the others.

Introducing one or more pointlike RTPs into (or instead of) a set of passive Brownian diffusers introduces two new dimensionless parameters. The first is the diffusivity ratio of passive to active species, $p = 2\gamma D/v^2$, which we always set to unity as stated previously. (This is purely to limit the scope of our study; the dependence on p is certainly interesting in principle.) The second is the number of environment particles per RTP run-length, $\tilde{\rho} \equiv \rho v/\gamma$. This physical density scale prevents us from absorbing ρ by a rescaling of time, as was possible for the all-passive cases in section 3.

Since we are not interested in either $\gamma \to \infty$ (a limit where RTP particles become Brownian) or $\gamma \to 0$ (where the RTP run length is infinite), then within the subspace $p = 1$ we can, without loss of generality, set $v = 1 = \gamma$ for all active particles present. This amounts to a specific choice of units of length and time, which we make from now on. In this case $\tilde{\rho} = \rho$; $D = 0.5$ and $t_{\mathrm{cr}}^{-1} = \pi\rho^2$ via equation (5). With these choices, the only physical control parameter stemming from activity is simply the density ρ. Alongside this we must retain as parameters N or L (governing finite size effects), and Δt (governing any time-discretization effects that might arise).

4.1. Active hardcore environments

We now address cases AxH, describing active and passive tracers in active hardcore environments, making comparisons between these and PPH.

4.1.1. AAH: active tracer in hardcore active medium. The AAH case describes a collection of $N + 1$ point RTPs with mutual hardcore exclusion, where the central particle is the tracer. Typical trajectories of seven consecutive hardcore RTPs (from the centre of a system with $N = 1000$) are shown in figure 4 (left). Like the PPH case in figure 3 these trajectories respect the no-crossing hardcore rule. However, in contrast to PPH, hardcore RTPs tend to stick to each other on contact. As discussed in section 2 above, this is due to their finite persistence time: when two RTPs meet head on, they remain stationary until one or both of them flip(s) direction.

The tracer variance $\mathrm{Var}(X)$ as a function of time is shown in figure 4 (right) for a system of $N = 2000$ with density $\rho = 10$. At early times, the tracer neither sees its neighbours, nor does it have a significant probability to flip its direction of motion. Thus it moves ballistically and $\mathrm{Var}(X) \sim t^2$. At times longer than the persistence time, $t > \gamma^{-1}$, the variance crosses over to the subdiffusive $\sqrt{t}$ scaling, as for PPH, but with a different prefactor, see section 4.1.3 below.

4.1.2. APH: passive tracer in hardcore active medium. Typical trajectories for five central particles in a system of $N = 1000$ hardcore RTPs, hosting a centrally placed diffusive tracer (black solid line), are shown in figure 5 (left). Once again the worldlines do not cross, in accord with the hardcore condition. However, the RTP particles tend to *travel together* for significant fractions of the time, including periods when they are static because one or more rightmoving particle lie(s) directly to the left of one or more left movers. Significantly, the passive tracer, while not directly subject to the same 'stickiness', can easily become trapped between either head-to-head or comoving RTPs, in which case its Brownian fluctuations are suppressed. On the other hand, there are also epochs where the tracer has a pair of static (head-to-head) RTPs on its left, well
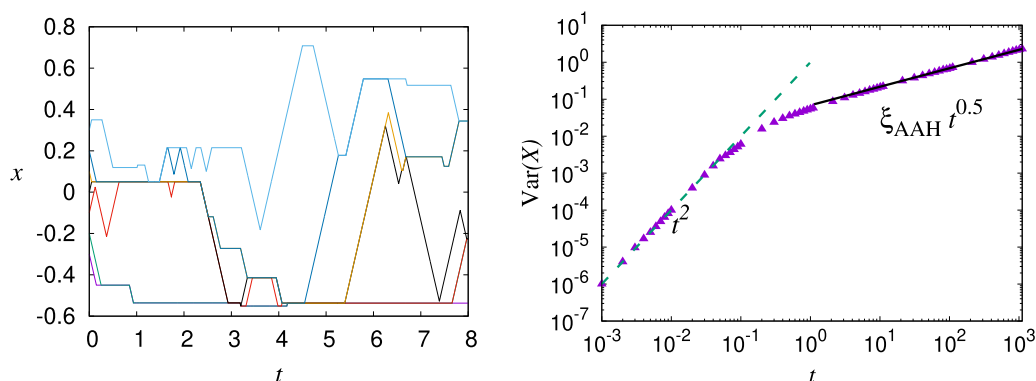
Figure 4. (Left) Typical AAH trajectories for seven consecutive hardcore RTPs (from a total of $N + 1 = 1001$ particles at $\rho = 10$; others not shown). (Right) $\mathrm{Var}(X)$ as a function of time t (purple triangles). Dashed line: t^2; solid line is the best $\sqrt{t}$ fit at late times, identifying the subdiffusion coefficient ξ_{AAH}. Points are simulation results. The $\sqrt{t}$ behaviour sets in at timescales $t > \gamma^{-1}$. Parameters are $\rho = 10, N = 2000$ and $\Delta t = 0.001$. Data averaged over 1.5×10^4 realizations. Length and time units are chosen so that $v = 1, \gamma = 1$ (see text); this silently applies also in all subsequent figures.
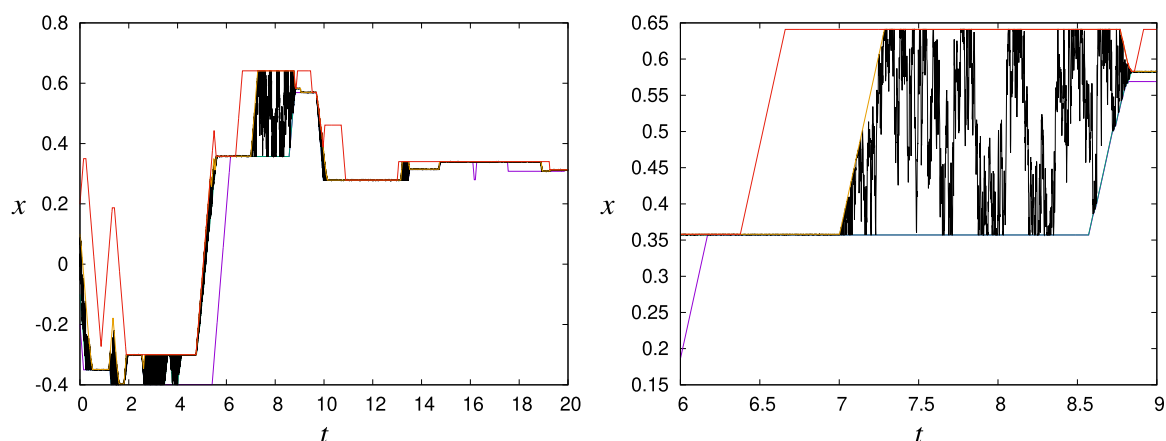
Figure 5. (Left) Typical trajectories for the central five particles in an APH system comprising $N = 1000$ RTPs and a centrally located passive tracer, at a density $\rho = 10$. (Right) Zoom-in on an episode of free tracer diffusion confined by two RTP particles that are each stationary because of a head-to-head encounter with another RTP. Simulation time-step $\Delta t = 0.001$.

separated from another pair on its right, in which case the tracer diffuses within this confining box, figure 5 (right).

Figure 6 plots $\mathrm{Var}(X)$ against time for the passive tracer in case APH, at density $\rho = 10$. At very early times the tracer is a free Brownian particle: $\mathrm{Var}(X) = 2Dt$. Upon encountering its RTP neighbours, which either move ballistically or are stationary until $t \gg \gamma^{-1}$, the diffusive tracer is slowed down drastically. This causes the plateau-like region in figure 6 and illustrates *transient caging* of a passive particle by its two active
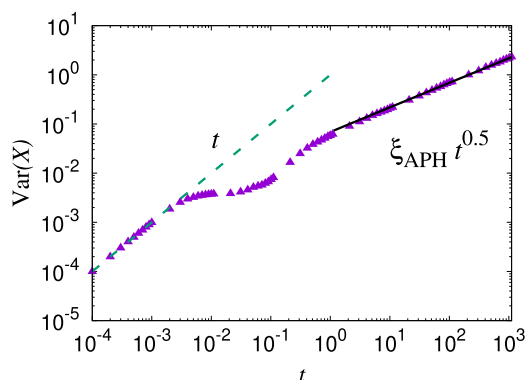
Figure 6. Tracer variance $\mathrm{Var}(X)$ as a function of time for APH (a passive tracer surrounded by hardcore RTPs) at density $\rho = 10$. Points represent simulation results. At late times, $\mathrm{Var}(X)$ approaches $\xi_{\mathrm{APH}}\sqrt{t}$. The subdiffusion coefficient ξ_{APH} is a best fit (solid line) to the late-time data. Parameters: $N = 2000, v = 1 = \gamma$, $D = 0.5$. $\Delta t = 0.0001$ for $t \leqslant 10$ and $\Delta t = 0.001$ for $t > 10$. (Overlap of data for both Δt values checked for t in the range [1, 10]. Smaller Δt value taken to extract early-time free diffusive behaviour of the passive tracer.) Data averaged over 10^4 realizations.

neighbours. The length of the plateau increases with the density of the bath particles, as the passive tracer then encounters its neighbours earlier but still has to wait until $t \sim \gamma^{-1}$ for a neighbour to flip before it can diffuse further. The end of the plateau at $t \sim \gamma^{-1}$ thus marks the end of an early time regime during which free diffusion and then caging have both occurred. (Note that this plateau indicates a *transient* caging effect, in that the size of the cage is primarily determined by the equispaced initial condition. If the mean-squared displacement is measured instead between times t_0 and $t_0 + t$ then the results depend significantly on the lag time t_0, see appendix C.)

   After escaping this transient cage, the tracer movement becomes strongly correlated with the environment particles; at late times, $t \gg \gamma^{-1}$, the latter increasingly resemble hard core diffusers like the tracer itself. Accordingly $\mathrm{Var}(X)$ scales as $\sqrt{t}$ as found for PPH (section 3). Similar to AAH, the coefficient of subdiffusion differs from the passive case, this is discussed next.

4.1.3. Subdiffusion in AAH, APH and PPH: a comparison. Figures 3, 4 and 6 show that $\mathrm{Var}(X) \sim \sqrt{t}$ at large times for each of PPH, AAH and APH. We understand this convergence of power laws by arguing that at late times $(t \gg \gamma^{-1})$ each RTP performs an effective diffusion between its neighbours; the microscopic details of individual particle motions get lost, and the RTP environment behaves as a diffusive fluid in the sense of MFT, as discussed in section 3. In this case the arguments of [4] provide a natural explanation of this subdiffusive behaviour. However, the collective diffusion of the active environment is not the same as for the passive case, so the coefficient of subdiffusion ξ differs. In figure 7, we plot ξ_{AAH} and ξ_{APH}, found by fitting the late time data to $\sqrt{t}$, as a function of ρ. These quantities precisely coincide with each other, but not with ξ_{PPH}. The fact that $\xi_{\mathrm{AAH}} = \xi_{\mathrm{APH}}$ is consistent with the idea that the tracer motion is controlled by the collective dynamics of the environment—this is essential for
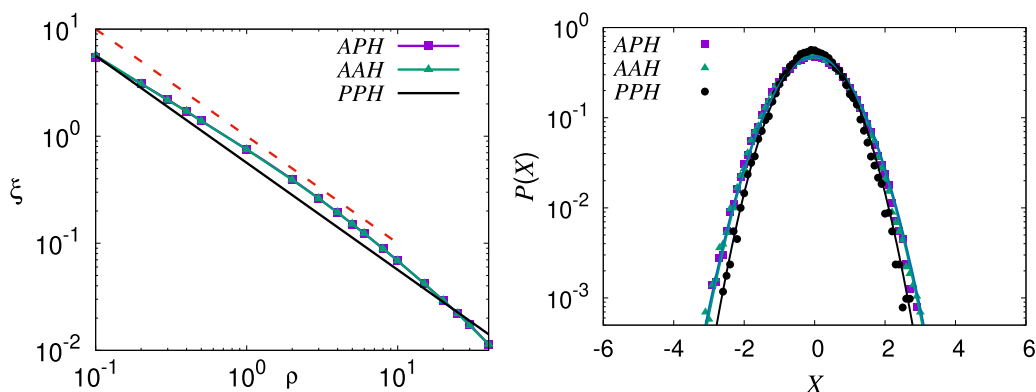
Figure 7. (Left) Comparison of simulation results for the coefficient of subdiffusion ξ in APH and AAH cases. $D = 0.5, N = 2000, v = 1 = \gamma, \Delta t = 0.001$. All data averaged over at least 1.5×10^3 realizations. Solid line: ξ_{PPH} from equation (4) with $D = 0.5$. Dashed line $\propto \frac{1}{\rho}$ is to guide the eye. (Right) Histogram (on a semi-log scale) of tracer position X at late time $t = 100$ with $\Delta t = 0.001$ and $N = 2000$ environment particles at initial density $\rho = 10$. AAH, APH and PPH data averaged over 8.6×10^4, 8.8×10^4 and 9×10^4 realizations, respectively. The solid lines (with the same colour codes as points) are Gaussian fits to each case with the respective variances calculated numerically.

the MFT analysis of [4] which relates the tracer motion to the environmental diffusivity and mobility. (We will show below that the PAH system differs strongly from AAH in this respect.)

Moreover, the deviation between PPH and AxH is not a constant multiplier, but instead a factor that itself depends on density, which presumably originates in the mobility and diffusivity of the active environment. Indeed from equation (4), $\xi_{\mathrm{PPH}} \propto \rho^{-1}$, and while this scaling is recovered for $\rho \ll 1$ (to be precise $\frac{\rho v}{\gamma} \ll 1$) where RTPs reach a diffusive limit before encountering any neighbours at all, the plot of $\xi_{\mathrm{AAH,APH}}(\rho)$ shows appreciable downward curvature throughout the studied range ($0.1 < \rho \leqslant 40$). This quantitative difference can be intuitively understood by considering the dimensionless quantity $\frac{\rho v}{\gamma}$ which can in turn be interpreted as a ratio of two competing timescales, $t_{\mathrm{flip}} = \frac{1}{\gamma}$ and $t_{\mathrm{int}} = \frac{1}{\rho v}$. The diffusive ($PPH$) limit is recovered when $t_{\mathrm{flip}} \ll t_{\mathrm{int}}$. For $t_{\mathrm{flip}} \sim t_{\mathrm{int}}$ ballistic hard-core collisions arise (and persistence comes into play) between RTPs before their diffusive regime gets established. If $t_{\mathrm{flip}} \gg t_{\mathrm{int}}$, the system will effectively be jammed for long observational time-windows (we do not access such limits in this paper).

Given these differences, it is notable that, as exemplified in figure 7, in the late time regime the distribution $P(X)$ for the AAH and APH cases is Gaussian (to within numerical error), just as it is known to be (exactly) for PPH [4]. The emerging picture is therefore of equivalence between these three cases at long times, up to a density-dependent renormalization of the coefficient of sub-diffusion in the hardcore active environment. This renormalized sub-diffusion coefficient that results from an interplay of the density ρ and the active run length $\frac{v}{\gamma}$ (or equivalently between t_{flip} and t_{int}), is a
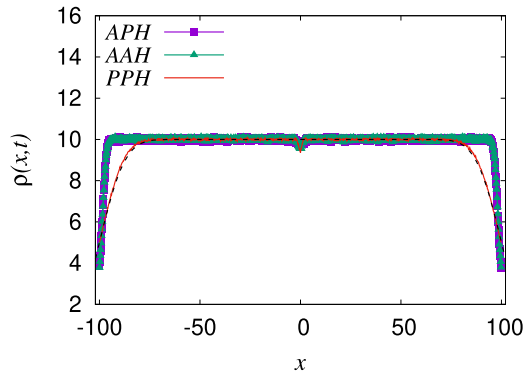
Figure 8. Density profile of environment particles ($N = 2000$) at a late time $t = 100$ for cases PPH, AAH, and APH. $v = 1 = \gamma, D = 0.5, \Delta t = 0.001$. Initially we have $L = 100$, therefore $\rho(x, t = 0) = 10$. While the AAH and APH density profiles are nearly indistinguishable, they are markedly different from the PPH profile. The PPH density profile converges on the result in equation (3) (dotted black line, mostly overlaying PPH data; also see figure 2). AAH, APH and PPH data averaged over 1.7×10^5, 1.6×10^5 and 5×10^4 realizations, respectively. The data was sampled only in the range shown in the plot.

collective effect and cannot be understood from a single-particle picture (as the interchanging worldlines argument for the PPH case also does not work for two hardcore RTPs). This reinforces the idea that in fully hardcore active systems the dynamics of a tracer is enslaved to the environment so that its own properties are almost immaterial. It is important to recall here the Percus relation which works quite generally for hardcore *passive* Brownian particles: the mean-squared displacement of a particle in the hardcore system is equal to the ratio of the average displacement of the corresponding free particle to the density of the hardcore environment [54, 55]. In an active environment composed of hardcore RTPs, we infer from figure 7 that the Percus relation no longer remains valid.

With this in mind, we now focus on the environment particles, to mechanistically elucidate the tracer statistics shown in figure 7. Density profiles of the environment particles are shown in figure 8 at a late time $t \gg \gamma^{-1}$, in the subdiffusive regime where $\mathrm{Var}(X)$ scales as $\sqrt{t}$. Consistent with our arguments, the results for the AAH and APH cases coincide, while the PPH density profile remains distinct. The latter matches equation (3) modulo a residual small dip at the origin (as the position of the tracer has been ignored). This outcome arises because, as discussed in section 3, the hardcore interaction does not alter the worldline statistics in a 1D gas of purely Brownian point particles.

However, this changes drastically for an environment comprising RTPs, whose orientational persistence can lead to jamming and causes nontrivial density correlations throughout the system. These correlations directly affect the late-time *collective motion* of the environment particles. For the chosen initial density ($\rho = 10$) in figure 8, we obtain a much slower spreading of the initial top-hat density profile when compared to *PPH* case. (This effect can be understood by considering the rightmost particle that

has orientation $\tilde{\sigma} = -1$: this particle acts as a (temporary) hard wall for the remainder of the particles, which tends to confine them, until such time as it flips its orientation. By contrast, passive particles are in constant diffusion motion, so they are much less effective in blocking other particles. This effect hinders spreading; it may be interpreted as a macroscopic analogy of the transient caging effect described above.)

We also note that while our AAH situation bears close resemblance to the single-file RTP system studied in [40], our point-like particles are strictly hardcore, in contrast to those of [40] where they have a finite interaction-range. Thus in our case, we do not have spatially extended clusters. Note also that the particles in [40] interact by physical forces within a Langevin description, which leads to significantly different dynamics for particle clusters, compared to this work (recall section 2). This, we believe, leads to a different scaling for our coefficient of sub-diffusion with density, as compared to the one in [40].

### 4.2. Active noninteracting environments

Having dealt with active hardcore environments we next address cases AxN in which the environment comprises active but noninteracting particles. (As always, the tracer has hardcore interactions with its environment and the active and passive diffusivities are matched.) We will make comparisons with the all-passive counterpart PPN—which as explained in section 3 is equivalent with PPH for our purposes.

The removal of interactions among active environment particles raises important questions. First, does the $\sqrt{t}$ law for the variance of a passive tracer continue to hold? Second, what if the tracer is itself active? And third, if the $\sqrt{t}$ law does hold, then how does the coefficient of subdiffusion get modified in each case?

4.2.1. Typical trajectories. To start to answer these questions, we show typical trajectories of environmental and tracer particles in AAN (figure 10) and APN (figure 11), preceded for comparison by the relevant passive benchmark PPN (figure 9). In each case we show results for two different densities, $\rho = 1$ (left panel) and $\rho = 10$ (right panel). As usual we give trajectories for a few ($n = 5$ or 7) particles from the middle of a larger ($N = 1000$) system with the tracer particle in the centre. Note however that these cease to be the middle n particles over time because the ordering of the particles is no longer fixed by the hardcore interaction: environment worldlines can cross each other (but of course *not* that of the tracer).

Interestingly, in the active environment, density has a more pronounced effect on both active and passive tracers, compared with PPN. That is, comparing figures 10 and 11 with figure 9, the tracers in the active environments make comparatively longer excursions at low environment density (left panels) but become nearly immobile for high density (right panels). This is because the active particles of the environment can stick to the hardcore tracer; an active tracer stops moving when head-to-head with an active environment particle whereas a passive tracer gets stuck between two head-to-head neighbours. As the density is raised, the probability of such encounters increases and the tracer's movement becomes more and more restricted. This effect is amplified by having free environment particles rather than hardcore ones, which would otherwise tend to arrest each other rather than the tracer (as discussed further below).
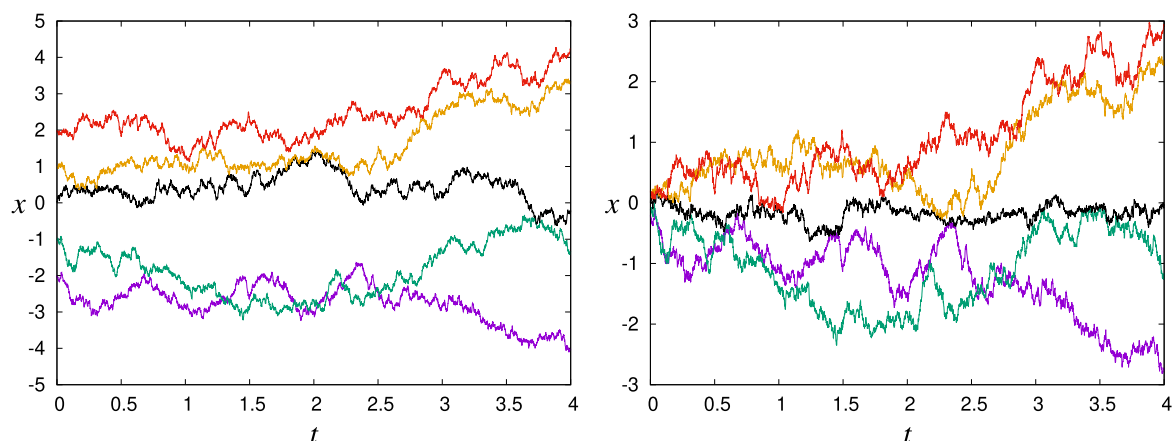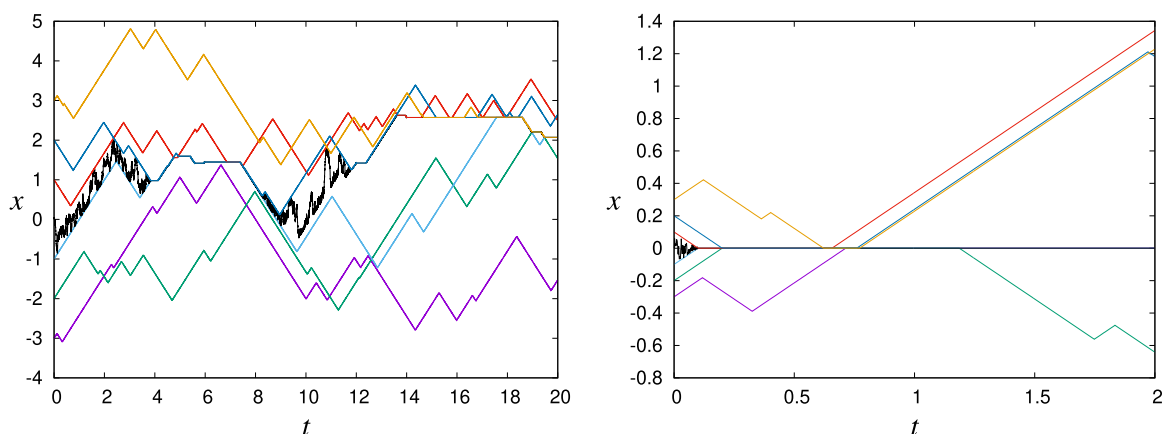
Figure 9. Trajectories for five central particles in the PPN case with $N = 1000$, $\Delta t = 0.001$, at density $\rho = 1$ (left) and $\rho = 10$ (right). The central black line is the tracer trajectory. Since the environment particles have zero persistence, the passive tracer is able to make large excursions, even at high density, unlike in dense active environments (compare figure 11 (right)).
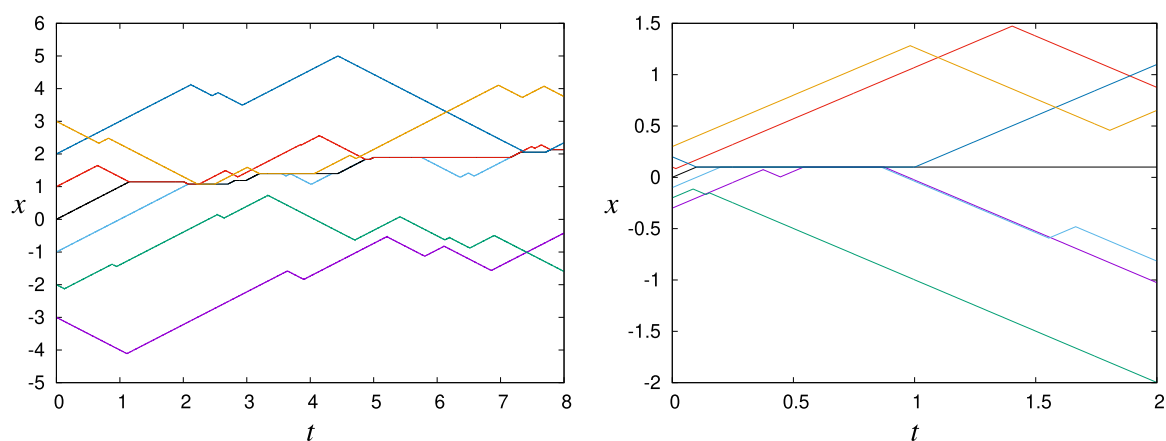

Figure 10. Trajectories for seven central particles in the AAN case with $N = 1000$, $\Delta t = 0.001$ at density $\rho = 1$ (left) and $\rho = 10$ (right). The central black line is the tracer trajectory. The active tracer can make long excursions at low environment density, but in a highly dense active environment (right), becomes increasingly immobile due to frequent encounters with another persistent particle.

4.2.2. Tracer variance. Figure 12 compares the time evolution of $\mathrm{Var}(X)$ in the AAN, APN and PPN systems, for two different densities. At very short times, the tracer does not interact with the environment so $\mathrm{Var}(X)$ scales diffusively ($\sim t$) for a passive tracer and ballistically ($\sim t^2$) for an active one. This changes as the tracer starts to interact with its neighbours; the higher the density, the sooner this is.

When the density is low, the late-time data for AAN, and APN coincide to numerical accuracy with PPN, which in turn is exactly governed by equation (4) for PPH as explained in section 3. Thus at low enough density the long-time subdiffusive tracer

Figure 11. Trajectories for seven central particles in the APN case with $N = 1000$, $\Delta t = 0.001$ at density $\rho = 1$ (left) and $\rho = 10$ (right). Similar to the AAN situation in figure 10, clustering of RTPs around the passive tracer makes it effectively immobile for long durations in dense active environments.
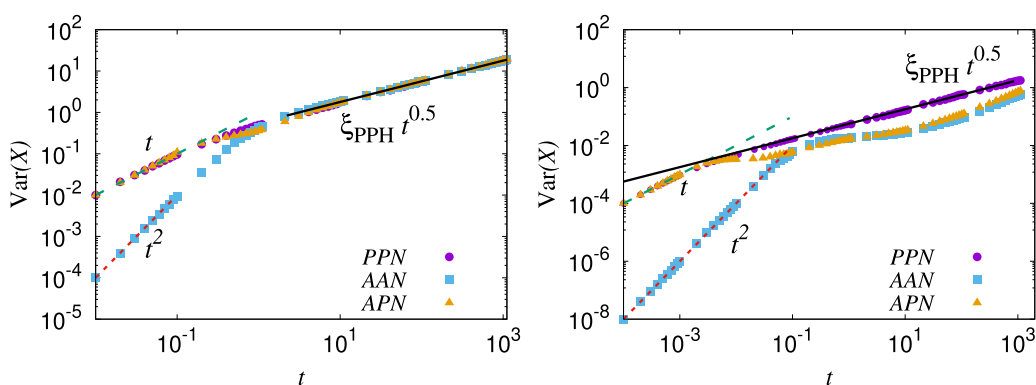
Figure 12. Time evolution of $\mathrm{Var}(X)$ for low (left panel, $\rho = 1$) and high (right panel, $\rho = 10$) densities. $N = 2000$ with $\Delta t = 0.0001$ for $t \leqslant 1$ and $\Delta t = 0.001$ for $t > 1$. (Overlap of data for both Δt values checked for t in the range [1, 10]. Smaller value of Δt taken to extract the early-time free diffusive behaviour of passive tracers.) All data averaged over at least 5×10^3 realizations. At low densities, in the long time limit, all cases coincide, with the same subdiffusion coefficient ξ_{PPN} (which is also exactly ξ_{PPH}, see section 3). At high density the active environments deviate from $\sqrt{t}$ behaviour for the observed time windows, owing to sticking of active particles to the tracers. We have truncated the data before finite-size effects can set in for the chosen value of N; see also appendix B.

behaviour is identical to the case of a passive diffusive environment, because any active particle (whether tracer or environmental) is already diffusive on the typical timescales of collision. Any tracer in such sparse active environments effectively sees a train of passive Brownian particles on either side, and therefore, both AAN and APN reduce to the PPN (and therefore PPH) case. The same argument applies in principle to hardcore
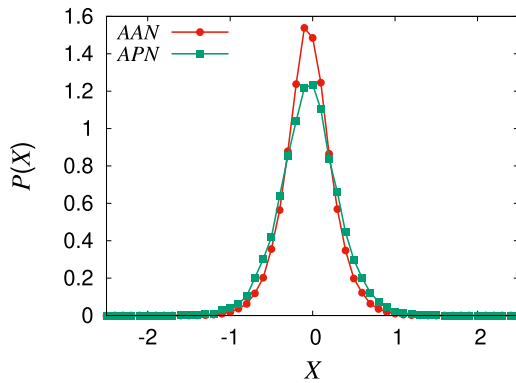
Figure 13. Histograms of the passive and active tracer-position X in the non-interacting active environment at time $t = 100 \gg \gamma^{-1} = 1$. The active tracer is more localized than the passive tracer in the same active environment. $N = 2000, \rho = 10$ and $\Delta t = 0.001$. Data averaged over 2×10^5 realizations.

active environments—but for these, as seen in section 4.1.3 above, $\rho = 1$ is not a low enough density to reach the *PPH* asymptote.

At the higher density, $\rho = 10$, case *PPN* continues to exactly track *PPH*, as it must, but significant deviations from this arise for both *APN* and *AAN*. The idea of swapping worldlines that lies behind the *PPH*–*PPN* equivalence of section 3 does not work for the persistent trajectories of RTP particles. The ultimate long-time behaviour remains open: in our simulations, before any convergence onto a subdiffusive, *PPH*-like behaviour at late times can be seen, finite-size effects (of the kind described in section 3.3 above) come into play. See appendix B for further discussion. Given the discussion above, it is plausible, but not certain, that in an infinite system the *AAN* and *APN* curves would asymptote from below towards the solid line, $\text{Var}(X) = \xi_{\text{PPH}}\sqrt{t}$, even though *AAH* and *APH* do not (see section 4.1.3 above). We return to this question in section 4.2.3 where a wider range of densities is addressed.

At $\rho = 10$, for both *AAN* and *APN*, there is a sustained region where $\text{Var}(X)$ falls well below the results for the passive environment, with no clean power law. As reported above for case *APH*, this indicates *transient caging* of the tracer particle by its active neighbours. Indeed the trajectory data of figures 10 and 11 show this caging effect directly. Interestingly, in contrast to the *AxH* cases (see figures 7 and 8), we find that at high density *AAN* and *APN* results do not generally coincide with each other in the long-time regime, $t \gg \gamma^{-1}$. This means that, unlike for the hardcore cases, the tracer dynamics is not fully enslaved to that of the surrounding environment in this regime. This mismatch between *AAN* and *APN* cases can also be seen from the respective tracer-position distributions, see figure 13. Note that in these cases the *only* interactions are those directly involving the respective tracers, in contrast to the hardcore active environment (AxH), whose multiple interactions correlate the tracer dynamics with $n \sim \rho(Dt)^{1/2}$ environmental particles. It is understandable therefore that in the hardcore active environment only, the dynamics of a lone tracer is eventually enslaved and its own character is forgotten.
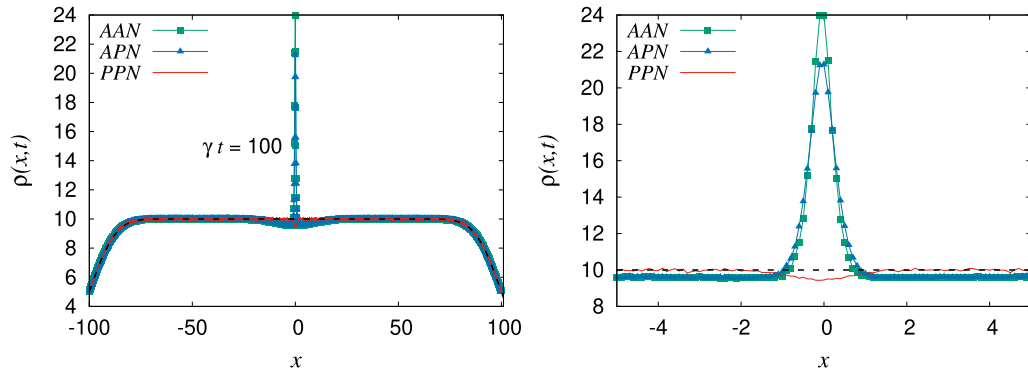
Figure 14. (Left) Density distribution of environment particles for a top-hat initial density of height $\rho = 10$ and $N = 2000$ (so $L = 100$) at time $t = 100$. $\Delta t = 0.001$; *PPN*, *AAN* and *APN* data averaged over 5.8×10^4, 3×10^5 and 3×10^5 realizations, respectively. Active particles of the medium cluster around both active and passive tracers. Dashed black line represents equation (3) for non-interacting passive Brownian particles. Data sampled only in the range shown in the plot. (Right) Zoomed-in version of the left panel. Though qualitatively similar, we observe more clustering for case *AAN* than for *APN*.

To understand better our results for the tracer variance $\mathrm{Var}(X)$ in dense active media, we show in figure 14 the density profiles of the environment particles around the tracer, sampled at a late time $t = 100$, for *AAN*, *APN* and, for comparison *PPN*. Far away from the tracer the density profiles are identical to statistical accuracy, and match the solution given in equation (3). This is as expected: particles sufficiently far away from a hardcore tracer do not feel its presence, and (whether active or passive) diffuse freely on these timescales. However, close to the tracer, we see that the active environment particles develop a pronounced density peak caused by sticking to the tracer via the mechanism described in section 2. The peak height differs somewhat between the cases of an active (*AAN*) and a passive (*APN*) tracer because the details of the sticking mechanism are tracer-dependent as described previously. There is of course no peak at all in *PPN* whose density, by the arguments of section 3, is oblivious to hardcore interactions either with the tracer or in the environment. We note here that our case *APN* and the problem studied in reference [47] both address a similar situation: a passive probe immersed in a sea of non-interacting RTPs. However, unlike [47] we consider a hardcore, pointlike tracer which leads to sub-diffusion in our model, but which is absent in [47].

4.2.3. Effects of density and ultimate long-time behaviour. So far we have looked at just two density values, $\rho = 1, 10$. At the higher of these, we did not observe $\mathrm{Var}(X)$ scaling as $\sqrt{t}$ within our investigated time-window. To clarify the long time behaviour we now study a wider range of densities, focussing on the *AAN* case. (The qualitative aspects are the same for *APN*.) In figure 15, we plot $\mathrm{Var}(X)$ against time for $\rho = 1, 2, 5, 10$. We observe that the $\sqrt{t}$ behaviour sets in later as the density of active particles is increased, preceded by the plateau-like region whose length increases with density. But only at the highest density does the final $\sqrt{t}$ regime fall entirely beyond
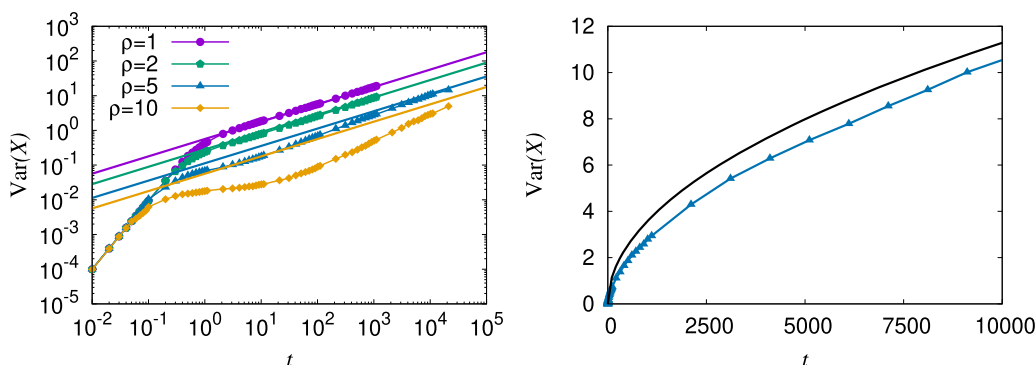
Figure 15. (Left) Time evolution of $\mathrm{Var}(X)_{\mathrm{AAN}}$ for various densities ρ. Points are simulation results. The free solid lines (with same colour codes as points) represent $\xi_{\mathrm{PPH}}\sqrt{t}$ for each density (and $D = 0.5$, equation (4)). Parameters $N = 8000$, $\Delta t = 0.01$. (Note that for cases AAx, long time results saturate already for $\Delta t = 0.01$ for our sequential updates). To observe $\mathrm{Var}(X) \sim \sqrt{t}$ at very high densities ($\rho \geqslant 10$) much larger time windows and larger number of particles would be required. We have truncated the data for $\rho = 5$ and 10 at a point where finite size effects set in. Number of realizations: 10^4 for $\rho = 1, 2, 5$ and 2×10^3 for $\rho = 10$. (Right) Time evolution of $\mathrm{Var}(X)_{\mathrm{AAN}}$ for $\rho = 5$ in the linear scale. Points represent simulation results for $N = 8000, \Delta t = 0.01$ and 10^4 realizations. The solid black line corresponds to $\xi_{\mathrm{PPH}}\sqrt{t}$, with ξ_{PPH} given by equation (4) (for $D = 0.5, \rho = 5$).

the observation window (which is limited by finite size effects as previously discussed). Based on this data, we expect there is no true breakdown of the relation $\mathrm{Var}(X) \propto \sqrt{t}$ in the ultimate long-time limit, so long as the limit $N \to \infty$ is taken first to avoid finite-size issues. Indeed such a breakdown would require some sort of critical density at which the asymptotic exponent changes value; we have found no evidence for this.

For a physical understanding of this AAN case, note that higher densities result in more environmental particles sticking to the tracer, flattening the plateau in $\mathrm{Var}(X)$ at intermediate times. At these times the active tracer is mainly trapped, and only freed by rare events in which *all* of the stuck particles on its forward side start moving away. This effect is even more pronounced at higher densities than considered here, when these individual events can appear as sudden jumps in the log–log plots unless there is sufficient averaging over runs.

4.3. Comparison of noninteracting and hardcore active environments

It is clear from figures 7 and 12 that $\mathrm{Var}(X)_{\mathrm{AAH}}$ and $\mathrm{Var}(X)_{\mathrm{AAN}}$ have generically different behaviour at equal density ρ, even at quite late times ($t \gg \gamma^{-1}$). Interestingly, depending on the density and time, $\mathrm{Var}(X)_{\mathrm{AAH}}$ can be larger than $\mathrm{Var}(X)_{\mathrm{AAN}}$. This disproves the idea that adding hardcore repulsions somewhere in the system will always slow the tracer motion; instead, since this also alters the statistics of sticking, more subtle factors can come into play. In particular, ξ_{AAN}, the coefficient of subdiffusion for the AAN case, appears from figure 15 (left) to be the same within statistical error as ξ_{PPN} and hence also ξ_{PPH} for low density ($\rho = 1$) as given in equation (4), but as the density increases,

ξ_{AAN} saturates to a value slightly less than ξ_{PPH} (see figure 15 (right)). This contrasts with ξ_{AAH} which is larger than ξ_{PPH} in this density range, see figure 7.

Likewise for general ρ and t, the tracer variances $\mathrm{Var}(X)_{\mathrm{APH}}$ and $\mathrm{Var}(X)_{\mathrm{APN}}$ are different in general. In fact, $\mathrm{Var}(X)_{\mathrm{APN}}$ shows the same qualitative behaviour as $\mathrm{Var}(X)_{\mathrm{AAN}}$, and remains less than $\mathrm{Var}(X)_{\mathrm{APH}}$ for intermediate densities. (We do not show these results separately.) To summarize: the subdiffusion constants for $\mathrm{Var}(X)_{\mathrm{AxH}}$ are generically larger than $\mathrm{Var}(X)_{\mathrm{AxN}}$ at intermediate density $0.2 \lesssim \rho \lesssim 15$.

4.4. Role of initial conditions

As noted above, all results presented so far are for an initial condition with equispaced particles, and the mean squared displacement $\mathrm{Var}(X)$ is measured between times 0 and t. By contrast appendix C discusses how the results (for active environments) are changed if one instead measures the mean squared displacement between times t_0 and $t_0 + t$, for some lag time t_0 (in particular $t_0 = 1$). This affects the transient caging behaviour at short and intermediate time, but the large-t behaviour is the same.

5. Results for active tracers in passive environments

Having reviewed the two passive-in-passive cases (PPx) in section 3, and explored the four cases (Axx) of active or passive tracers in active environments with and without hardcore forces in section 4, there remain two cases so far unexplored in table 1. These are PAH and PAN, respectively describing an active RTP tracer surrounded by free or hard-core passive Brownian particles. In this section we show how the qualitative behaviours of PAH and PAN are similar to each other, but differ substantially from all the other cases presented so far.

Typical trajectories for the two cases are shown in figure 16, for seven central particles, including the active tracer, in the middle of a large system ($N = 1000$). These show qualitatively similar tracer motion although the environment worldlines differ considerably due to the presence (in PAH) or absence (in PAN) of the no-crossing constraint among them. (As always, no particle can cross the tracer.)

To explain why these active-in-passive systems are different from the other cases considered so far, we note from section 2 that a purely ballistic tracer moving with speed v moves freely, unless it encounters a particle within a distance $v\Delta t$. A low density environment of passive particles will slightly reduce the mean forward speed but this effect is small unless the (local) density is of order $(v\Delta t)^{-1}$. However, when a ballistic tracer moves forward in such an environment, it tends to accumulate a pile of passive particles in front of itself, by a 'snowplough' effect. This acts to increase the local density in front of the tracer, which may eventually exceed $(v\Delta t)^{-1}$, even if the average density of the system is small. We will show that this leads to results that depend significantly on the parameter Δt of our numerical algorithm, in contrast to active-in-active systems. (While this argument assumes a perfectly ballistic tracer, it is also relevant for RTP tracers, if the run length is long enough that the pile of passive particles has time to form between tumbles. Note that a pile-up of passive particles in one dimension due to *driven* (not active) tracers were discussed earlier in [56, 57].)
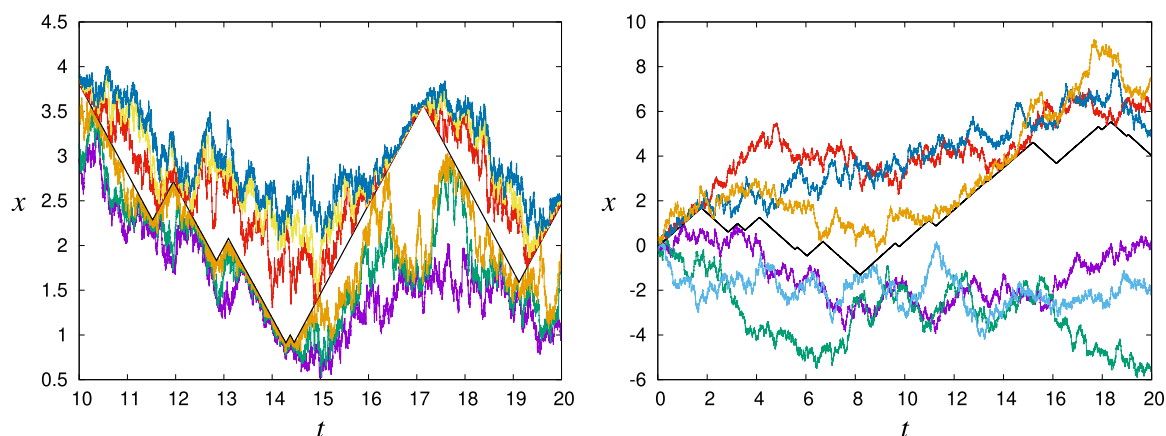
Figure 16. Trajectories for seven central particles in the *PAH* (left) and *PAN* (right) cases; $N = 1000$ and $\rho = 10, \Delta t = 0.001$. The central black line represents the RTP tracer. The active tracer often creates a *snowheap* of passive particles in front of itself.

It is important for this argument that if a passive particle encounters the active tracer, it reflects from it as described in section 2, so there is almost always some space ahead of the tracer, and it continues to make progress. For *PAH* the passive neighbours are also restricted by their own hardcore passive neighbours. In *PAN* this restriction is lifted and the tracer has comparatively more freedom to move forward.

To illustrate this effect, the time evolution of the density of passive particles around an active (RTP) tracer is shown in figure 17 for *PAH* and *PAN*. At very short times the tracer is ballistic, and non-interacting. However as it encounters the environment, the tracer continues to move ahead, creating a pile of passive particles in front of itself, just as a purely ballistic particle would. This continues until $t \sim \gamma^{-1} = 1$ when the tracer flips direction. It then pushes the passive particles that were previously *behind* it, until it flips again. Thus the tracer keeps piling up passive particles on both sides and shunts them away from its initial position. The flipping of the tracer also allows each passive pile to spread diffusively half the time. Accordingly, after $t \sim \gamma^{-1}$, the density peaks broaden in time without decreasing in mass (this argument neglects finite-size effects, as usual).

It is clear from figure 17 that the tracer particle strongly perturbs the environmental density around it—so tracer motion is not enslaved to its environment. This breaks the argument of [4] that subdiffusion should be generic in single-file systems, which explains the qualitative difference between *PAx* and the other cases considered so far. An MFT description of the *PAH* system might still be possible, but it would require that the ballistic motion of the tracer (between tumbles) is explicitly accounted for, to capture the effect of the tracer on the environmental density, recall [56, 57].

5.1. Parameter Δt sensitivity

For active tracers in passive media, the sensitivity of the snowplough effect to the particle step size $v\Delta t$ means that long-time observables likewise depend on Δt. This is illustrated
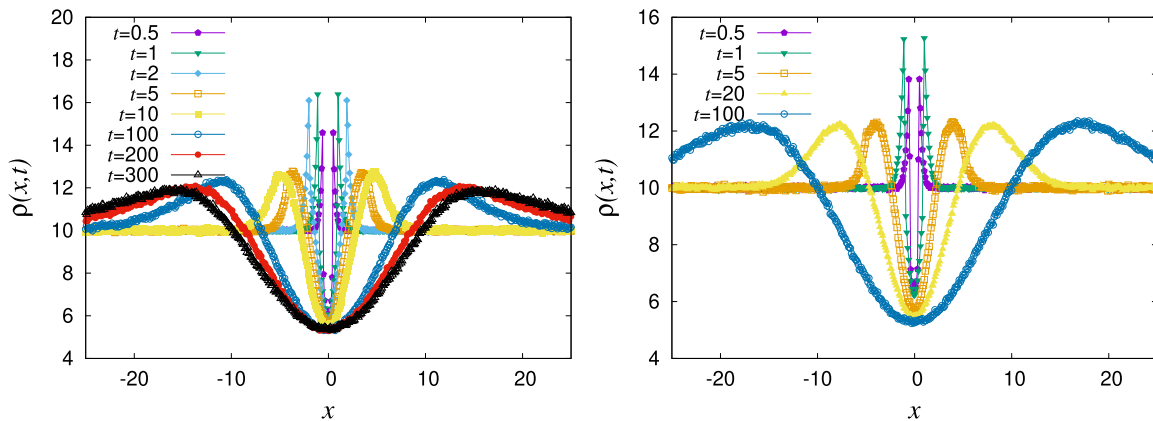
Figure 17. Time evolution of average density profiles around the tracer for PAH (left) and PAN (right). $N = 2000, L = 100, \Delta t = 0.001$. All $PAH(PAN)$ data averaged over 1.3×10^4 (2.5×10^4) realizations or more.

in figure 18 for the density ρ of environmental particles. Also, figure 19 shows $\mathrm{Var}(X)$ as a function of time with different values of Δt, for PAH and PAN. For small enough time-step the tracer variance crosses from ballistic at short times ($t \ll \gamma^{-1}$) to diffusive or near-diffusive behaviour at longer ones[3].

The PAH data are consistent with a scenario in which the mounds of passive particles ultimately slow the active tracer down to a subdiffusive $t^{1/2}$ behaviour, which sets in beyond a crossover time $t_{\mathrm{sub}}(\rho, \Delta t)$ that decreases with the density ρ. However, smaller timesteps Δt result in larger t_{sub}, which suppresses the subdiffusive regime. To see this regime clearly for $\Delta t \leqslant 10^{-4}$ might require very long observation times, in turn demanding much larger system sizes N to ensure that finite size effects are pushed out to $t \gg t_{\mathrm{sub}}$. The ultimate behaviour at $\Delta t \to 0$, $N, L \to \infty$ at fixed $\rho > 0$, and $t \to \infty$ remains open, and may depend on the order in which these limits are taken. Subdiffusive scalings for $\mathrm{Var}(X)$ are harder to reach in simulations for lower densities than those shown in figure 19. We do not show those results here.

We observe very similar trends on varying Δt for PAN; the data is also broadly consistent with the scenario elaborated in the preceding paragraph. Comparing the two cases at the same density and at the same (large enough) timestep, the active tracer to moves further in the non-interacting environment (PAN), compared to PAH. Figure 20 compares the two density profiles involved and shows more space for tracer motion in the PAN case, indicating (perhaps unsurprisingly) that it is harder for the active tracer to push a collection of hardcore particles than noninteracting ones.

5.2. Role of update rule

All results shown above for PAH and PAN were obtained with cyclic sequential Monte-Carlo updates as explained in section 2. Unlike for the other models, switching to a

---

[3] In contrast to these two active-in-passive cases (PAx), the dependence of $\mathrm{Var}(X)$ on the time-step (and also on the update scheme, see below) becomes minimal beyond $\Delta t \sim 10^{-3}$ or 10^{-4}, for fully active (AAx) and fully passive (PPx) cases respectively.
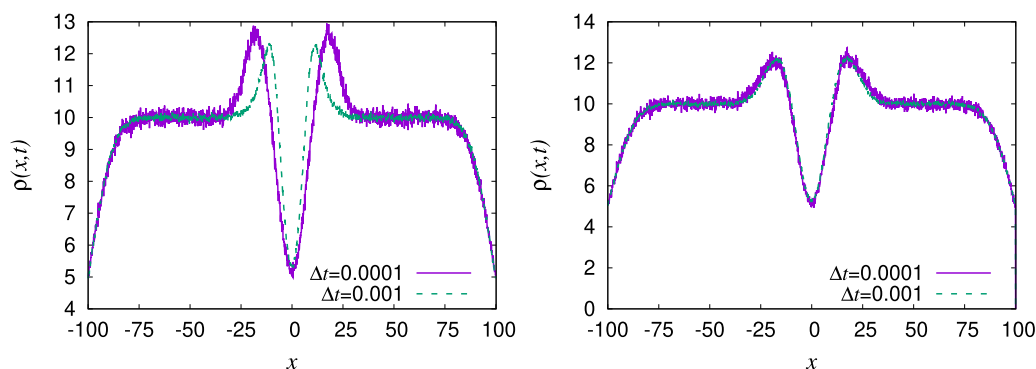
Figure 18. Effect of time-step Δt on environment particles in cases PAH (left) and PAN (right). Plot of the density profile of environment particles at a late time $t = 100 \gg \gamma^{-1} = 1$. We have $N = 2000$ passive particles with $L = 100$. For PAH, the $\Delta t = 0.001$ data is averaged over 2.3×10^4 realizations, while that corresponding to $\Delta t = 0.0001$ is averaged over 5000 realizations. For PAN, $\Delta t = 0.001$ data is averaged over more than 2.6×10^4 realizations, while for $\Delta t = 0.0001$, 3.5×10^3 realizations have been used. Other parameters are $v = 1, D = 0.5$. For smaller Δt, the active tracer accumulates a more massive snowheap of passive particles on either side. For the chosen values of t and Δt, this effect is pronounced for the PAH case and hardly any difference is observed for PAN. To observe the Δt sensitivity for PAN one needs either larger t or Δt; see figure 19 in similar context. Data sampled only in the range shown in the plots.

random sequential scheme (which is more prone to numerical diffusion), leads to significant quantitative changes in the time evolution of $\mathrm{Var}(X)$ in both these cases. However, the qualitative trend with respect to Δt is independent of the update rule chosen. This issue is discussed further in appendix A.

5.3. Further comparisons

At long times $t \gg \gamma^{-1}$, the density footprints left by an active tracer on passive environments are very different from those it leaves on active environments. In figure 21 (left) we compare the various hardcore density profiles for $\gamma t = 100 \gg 1, \rho = 10, \Delta t = 0.001$. In the passive environments, the active tracer shows a much larger displacement variance, with more freedom to move around in the 'correlation hole' created by pushing the environment particles into mounds further away. This is also seen from figure 22 where the tracer position distribution $P(X)$ is compared for all the four hardcore environments at $\rho = 10, \Delta t = 0.001, t = 100$.

From figures 21 and 22, it is clear that PAH is qualitatively distinct from the other three xxH cases due to the correlation hole/snowplough effect at large enough Δt. Similar analysis holds for PAN, see figure 21 (right); the active tracer is more efficient in pushing passive particles away (PAN) than active ones (AAN) and enjoys much larger freedom of movement as a result. The same figure also shows the separate phenomenon of sticking of the active environment particles to the tracer in the two AxN cases, as was already discussed in relation to figure 17.
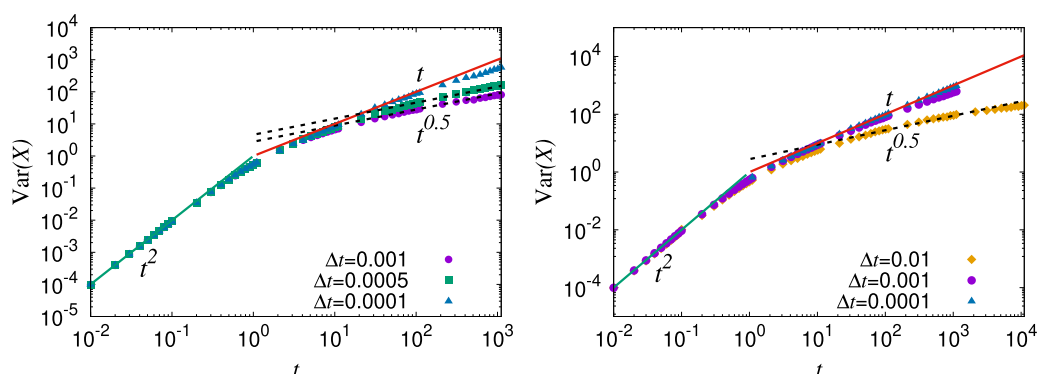
Figure 19. Tracer variance $\mathrm{Var}(X)$ as a function of time in *PAH* (left) and *PAN* (right). $N = 2000$, $\rho = 10$. Points are simulation results. At short times the tracer is ballistic. For very small $\Delta t\ (= 0.0001)$ the tracer shows nearly free diffusive behaviour at moderately long times for both *PAH* and *PAN* cases. For *PAH*, as Δt is increased, $\mathrm{Var}(X)$ starts to show $\sqrt{t}$ scaling behaviour instead ($\Delta t = 0.0005, 0.001$). Within the time-window of observation, $\Delta t = 0.001$ is not large enough to reach $\sqrt{t}$ scaling for *PAN*, although subdiffusive behaviour starts to appear at late times. $\Delta t = 0.01$ indeed shows close to $\sqrt{t}$ scaling for $\mathrm{Var}(X)$, but we suspect such a large value of Δt can be prone to errors for interacting passive Brownian particle-simulations. Number of realizations: PAH—4.5×10^3 for $\Delta t = 0.001$, 2.3×10^3 for $\Delta t = 0.0005$ and 500 for $\Delta t = 0.0001$; PAN—2.5×10^3 for $\Delta t = 0.01$, 5000 for $\Delta t = 0.001$ and 500 for $\Delta t = 0.0001$.
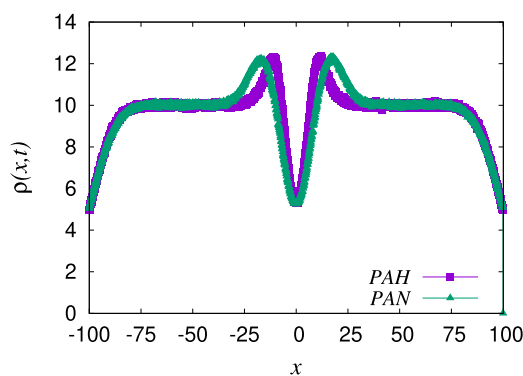
Figure 20. Average density profiles for bath particles in the *PAH* (2.3×10^4 realizations) and *PAN* (2.6×10^4 realizations) cases at time $t = 100 \gg \gamma^{-1} = 1$ with $\Delta t = 0.001$, $N = 2000$, $L = 100$. Data sampled only in the range shown in the plot.

6. Further discussion of clustering, sticking and caging

At high densities we have observed two distinct clustering effects caused by activity, neither of which occurs in the purely passive systems (*PPx*) that were extensively studied in previous literature. The first effect arises in the case of noninteracting active envi-
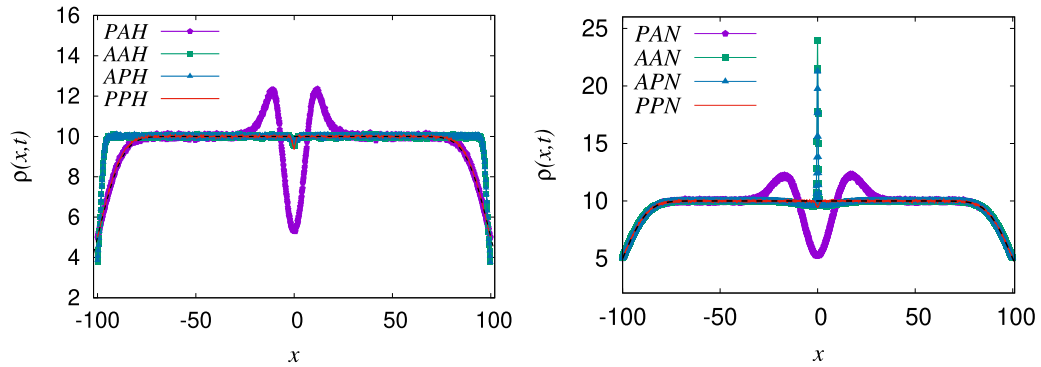
Figure 21. Density profile of environment particles at a late time $t = 100 \gg \gamma^{-1} = 1$, for hardcore (left) and noninteracting (right) environments. For both panels $\Delta t = 0.001$, initial density $\rho(x, t = 0) = 10$ with $N = 2000, L = 100$. At late times, while the AAH and APH density profiles are nearly indistinguishable, they are markedly different from the PPH and PAH profiles. AAN and APN density profiles show clustering of active particles around the initial position of the tracer, while PAN and PAH profiles show heaps of passive particles displaced by active tracers. The dashed black line in each panel represents equation (3) which coincides neatly with PPH/PPN data (barring the residual small dip at the origin, see section 4.1.3). AAH, APH, PAH and PPH data are averaged over $1.7 \times 10^5, 1.6 \times 10^5, 2.7 \times 10^4$ and 5×10^4 realizations, respectively. PAN data is averaged over more than 2.6×10^4 realizations. AAN, APN and PPN data are the same as used in figure 14. Other parameters are $v = 1, D = 0.5$. Data sampled only in the range shown in the plots.

ronments (AxN), and is caused by an accumulation of stuck particles around an active or passive tracer (figure 14 (right)). This type of pile-up is a somewhat universal phenomenon and also seen where free active particles impact on static boundaries [38, 58]. Interestingly, in our context at least, it is suppressed by hardcore interactions among the environment particles, mainly because these spend too much time sticking to each other to build up a high density next to the obstacle[4]. (This might well change in dimensions higher than one). A very interesting consequence is that, as seen in section 4.3, by making the environment more uniform, the introduction of hardcore interactions to an active environment tends to speed up, rather than slow down, the tracer dynamics.

The second type of clustering is the formation of 'snowheaps' of passive environment particles on either side of an active tracer in both PAH and PAN. For reasons we have described, these effects strongly depend on the discretization time-step and, to a lesser extent, on the update sequence (random vs cyclic). In this sense such effects are much less universal than those related to stuck particles. Nonetheless, both types of density inhomogeneity represent interesting signatures of activity that could be the focus of experimental attention. Importantly though, activity alone is not enough to see these inhomogeneities: neither effect is seen for AAH or APH.

---

[4] Note that motility-induced phase separation (MIPS) does not arise for our hardcore active environments at the densities and timescales considered here. If present, it would surely cause non-Gaussian statistics for $P(X)$, e.g. a superposition of two Gaussians corresponding to the two coexisting densities in the phase separation, in contrast to figure 7.
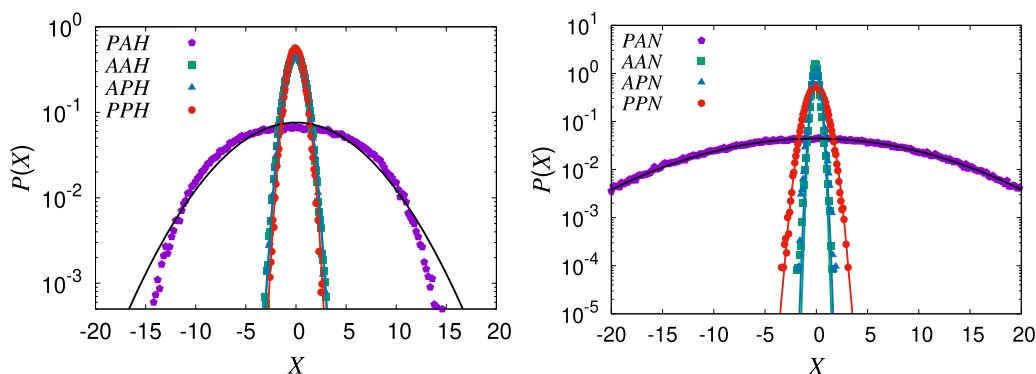
Figure 22. Histogram of tracer position X at late time $t = 100$ in different hard-core environments ($N = 2000, \rho = 10, \Delta t = 0.001, v = 1 = \gamma, D = 0.5$) on a semi-log scale. (Left) XXH and (right) XXN. PAX cases have much larger variances compared to the other six situations of table 1. Solid lines (black: PAX, red: PPX, blue: APX and green: AAX) represent Gaussian fits with the respective variances calculated numerically. PPH, AAH and APH data are the same as used in figure 7 (right). PAH data is averaged over 1.5×10^5 realizations. AAN and APN data are the same as used in figure 13. PPN and PAN data are averaged over 10^5 and 1.7×10^5 realizations, respectively.

Via the snowplough effect, the presence of an active RTP in a crowded passive environment also speeds up the transport of passive particles, at least at early times while the two 'snowheaps' are being created by the ballistic tracer dynamics. This may be related to the fact that mixtures of active and passive particles can optimize certain first passage properties in the cytoplasm, as reported in [59, 60].

The trapping of an active or passive tracer in an environment of dense non-interacting active particles bears comparison with glassy systems, where a tagged particle with early time ballistic motion undergoes dynamic arrest at intermediate timescales due to caging, before eventually showing diffusive behaviour [61, 62]. A related connection between active and glassy dynamics in dense systems was previously reported in [63]; also see [64] for links between activity-induced fluctuations and caging phenomenon in living cells. These links between hardcore tracer dynamics in single-file active environments and in glasses might be further interrogated by studying standard observables such as the pair-correlation function, but this lies beyond the scope of the present paper. Our results might also be relevant for studies on bacterial cytoplasm where dynamical arrest has been observed by monitoring the mean-squared displacement of cytosolic components [67].

7. Summary

We have studied the behaviour of tracers in hardcore interacting and non-interacting media in one-dimension for all eight combinations (table 1) of active and passive tracer and environment particles. The interaction between tracer and environment is always via

hardcore exclusion. Our active particles are point RTPs of velocity $\pm v$ and tumble rate γ (both taken as unity without loss of generality by choice of space and time scales) while our passive particles are point Brownian diffusers of free diffusivity $D = v^2/2\gamma = 0.5$ chosen to match the long-time behaviour of a free RTP. The initial configuration is such that all particles are equispaced, often called a 'quenched' initial configuration [4, 50], with random assignment of the orientation of each RTP. For each case we investigated the statistics of the tracer displacement (through its variance $\mathrm{Var}(X)$) and the environmental density profile around the tracer.

In active hardcore environments we observed late-time subdiffusive scaling for AAH and APH scenarios with a shared prefactor, $\mathrm{Var}(X) \to \xi_{\mathrm{AxH}}(\rho)\sqrt{t}$. The identical prefactor is explained by enslavement of the tracer to the active interacting environment. This prefactor does not however coincide with that known for a passive tracer in a passive environment, $\xi_{\mathrm{PPH}}(\rho) = \xi_{\mathrm{PPN}}(\rho) = (2D/\pi)^{1/2}\rho^{-1}$, under similar initial conditions. Note that *only* in the all-passive case are the noninteracting and hardcore environments automatically equivalent for tracer dynamics, via the worldline-swapping argument of section 3. Nonetheless, the density of environment particles around the tracer remains almost uniform in both AAH and APH.

In non-interacting environments at low enough density, the results for PPN, AAN and APN results merge at long times: $\mathrm{Var}(X) \to \xi_{\mathrm{PPN}}(\rho)\sqrt{t}$. This is because at low enough density, encounters between particles occur on a timescale beyond the flip time γ^{-1} of an RTP which has therefore effectively become Brownian. In contrast, for highly dense non-interacting active environments, any $\sqrt{t}$ regime recedes beyond our observable time windows (as set by finite size effects), for both active and passive tracers. This is a consequence of clustering of stuck RTPs around the hardcore tracers, which leads to caging and narrower displacement distributions. Moreover, in dense active environments, long time results for the active and passive tracers do not coincide, in contrast to what we found in hardcore environments at all densities.

The statistics of active tracers in passive environments (PAH and PAN) show a lower degree of universality than all other cases, and—at least in our implementation of the dynamics—depend strongly on the particles' step size $v\Delta t$. At small enough Δt, the PAH tracer shows nearly normal-diffusive behaviour for quite long times, and subdiffusive behaviour appears only much later (if at all) compared to the other three hardcore scenarios. Increasing the time-step leads to faster arrival of the subdiffusive regime. At equal density and time-step, the active tracer moves further in a noninteracting passive environment than an interacting one, reflecting the relative ease with which the environment particles can be gathered into mounds by a snowplough effect (operating during each ballistic 'run' of the RTP), thereby creating space for the tracer to move.

While we have studied all eight cases numerically, obtaining analytical solutions for the six that involve active particles offers a rich source of challenging open problems, to match those already addressed in purely passive systems (see [4]). We expect standard MFT techniques, in principle, to work for cases AxH (as the tracer remains slaved to the

environment) [4]. However, cases AxN and PAx require much more careful analytical treatments. A direct extension of our work would be to calculate current fluctuations through the initial tracer position for both interacting and non-interacting active environments. Whether or not one observes dynamical phase transitions in these set-ups remains an interesting question for the future. While our study is restricted to the case of matched diffusivities, relaxing this restriction could yield a range of further interesting regimes particularly when the mismatch becomes strong. Further, connections between tracer dynamics and interface growth models [65] in interacting active systems need to be investigated by applying an external bias on both the tracer and the environment. Also, how correlations between particle positions in single file active systems get affected by a *local* bias [66], remains a question for the future.

Although this paper focuses entirely on simple 1D models, the results presented here, include qualitative predictions about eventual subdiffusion, density anomalies, caging at intermediate times, and other activity-induced effects upon single-file diffusion. These might inspire and inform the future experimental exploration of systems with various probe/environment combinations such as *in vitro* set-ups mimicking transport processes in the bacterial cytoplasm [67], or a passive probe placed within an active bacterial culture [68, 69].

## Appendix A. Comparison of update rules

Here we compare $\text{Var}(X)$ results for some of the cases in table 1 found through the cyclic sequential update (detailed in section 2), denoted S, with those from a random sequential update scheme, denoted RS.

For the RS scheme, each simulation time-step, we draw $N+1$ (bath particles + tracer) integer random numbers between 1 and $N+1$. Whichever value the random number takes, we update the particle with that index. The rest of the algorithm is exactly similar to the one described in section 2. Here we summarize the comparisons:

- AAH: figure A1 (left) shows excellent agreement of S with RS for $\Delta t = 0.001$.
- AAN: figure A1 (right) shows excellent agreement of S with RS for $\Delta t = 0.001$.
- PPH: figure A2 (left) shows a good agreement of S with RS for $\Delta t = 0.0001$.
- PAH: figure A2 (right) shows a mismatch at moderately late times between S and RS for both $\Delta t = 0.0001$ and $\Delta t = 0.001$. However, the trend that $\text{Var}(X)$ shows with respect to Δt is the same for both schemes.
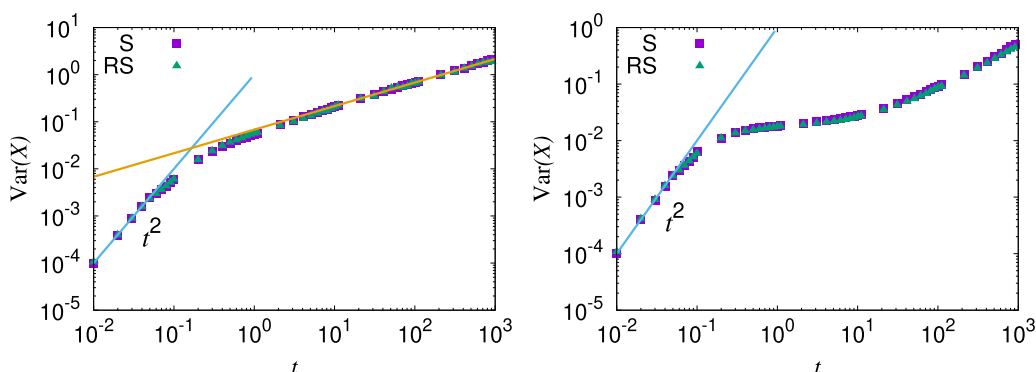
Figure A1. $\mathrm{Var}(X)$ as a function of time, comparing S and RS updates for the AAH (left) and AAN (right) cases. The yellow line is a fit of $\sqrt{t}$ to the late-time data. $N = 2000, \rho = 10, \Delta t = 0.001$. For AAH, S data is averaged over 1.5×10^4 realizations and RS data over 7×10^3 realizations; for AAN both data sets averaged over 7×10^3 realizations. For both panels $v = 1 = \gamma$.
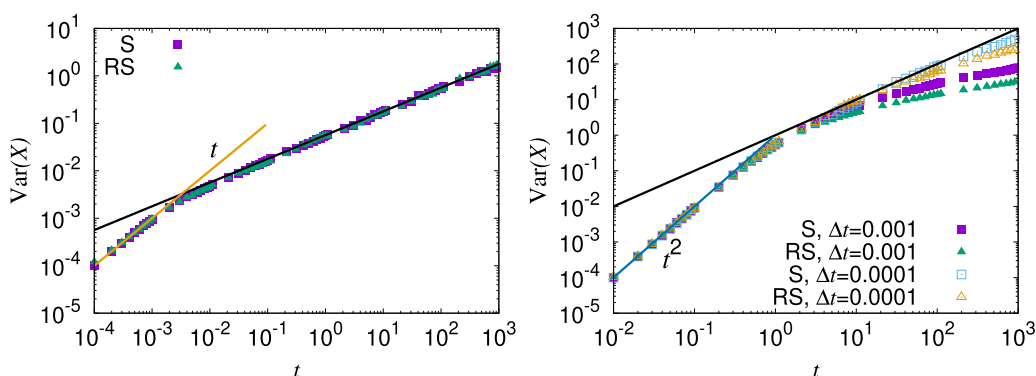
Figure A2. $\mathrm{Var}(X)$ as a function of time, comparing sequential (S) and random-sequential (RS) updates for: (left) the PPH case (S data same as in figure 3 (right)); RS data over 400 realizations. Solid black line is equation (4). $N = 2000, \rho = 10, \Delta t = 0.0001, D = 0.5$. (Right) the PAH case. Solid black line is $2Dt$. $N = 2000, \rho = 10, v = 1 = \gamma, D = 0.5$; various Δt as given in legend. RS data for $\Delta t = 0.001$ averaged over 3.5×10^3 realizations and $\Delta t = 0.0001$ over 350 realizations. S data is the same as in figure 19 (left).

Appendix B. Finite size effects: illustrative results

Here we investigate the finite-size effect on the late-time tracer dynamics stemming from the finite number of environment particles. Figure B1 (left) illustrates the finite-size-induced restoration of linear scaling for $\mathrm{Var}(X)$ vs t at very late times for a system with $N = 500$ particles in the PAN, AAN and APN cases, as discussed in sections 3.3 and 4.2.2. In figure B1 (left), we see that finite size effects are visible in the turn up of the PPN data which then lie above the exactly known result $\mathrm{Var}(X) = \xi_{\mathrm{PPH}}\sqrt{t}$ (solid line). The latter holds only for $N \to \infty$ and this mismatch is exactly as expected from
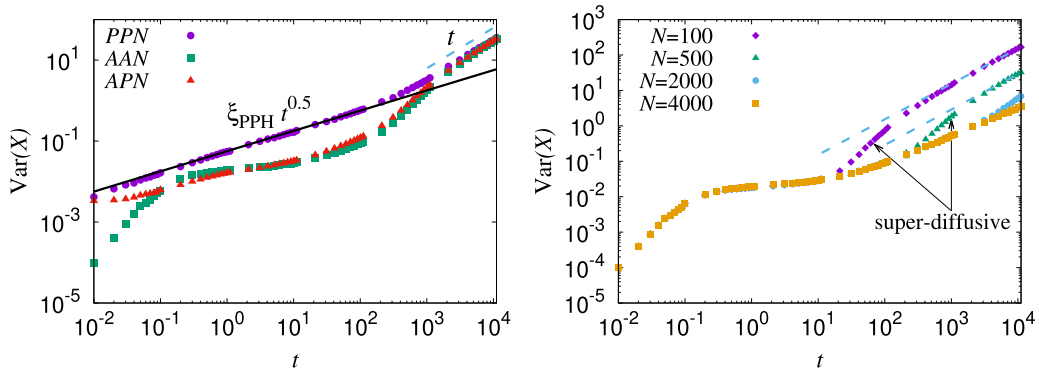
Figure B1. (Left) $\mathrm{Var}(X)$ for various tracers in different non-interacting environments for a high density, $\rho = 10, N = 500, \Delta t = 0.001$. Finite size effects cause a crossover back to linear scaling of $\mathrm{Var}(X)$ (dashed line). Black solid line is equation (4). (Right) $\mathrm{Var}(X)$ against time in the AAN case for different N, with $\rho = 10$ and $\Delta t = 0.001$. Dashed lines show linear scaling. All data sets averaged over a minimum of 7×10^3 realizations.

the arguments given in section 3.3. The same arguments apply equally to the APN and AAN curves which therefore also turn up cross the solid line (but not the actual PPN data).

In figure B1 (right), we systematically vary N and focus on the AAN scenario with $\rho = 10$. For small system sizes ($N = 100, 500$), we observe that $\mathrm{Var}(X)$ leaves the plateau and becomes superdiffusive before showing diffusive behaviour. It is notable that similar evolution for mean-squared displacements with a caging regime followed by superdiffusive and diffusive regimes has been reported in passive colloidal systems under shear [70] or for crowded systems involving active Brownian particles [71]. The apparently 'superdiffusive' catch-up region of very high positive slope ($\mathrm{d}\ln\mathrm{Var}(X)/\mathrm{d}\ln t \gg 1$), as far as we can tell, is not physically significant: plotting instead $\mathrm{Var}(X)$ against $\sqrt{t}$ on linear axes will show a simple crossover from the constant plateau to a linear late time regime. We do not attach direct physical significance to the superdiffusive regime for the problems studied here.

Appendix C. Role of delaying the start of observations

All results in the main text were obtained with the time interval between preparation of the equispaced initial state and the start of observations to be zero. We now introduce a *lag-time* t_0 between the preparation of the initial equispaced state and the onset of observations for a given initial density $\rho = 10$. The tracer's displacement X is then measured from its value at $t = t_0$. The variance of X is then given by

$$\mathrm{Var}\left(X\right)_{t_0} = \langle [X(t_0 + t) - X(t_0)]^2 \rangle - \langle [X(t_0 + t) - X(t_0)] \rangle^2. \tag{C.1}$$

We show results for AAH and APH (figure C1 (left)) and for AAN (figure C1 (right)). We observe that the late-time results remain independent of the choice of t_0. However, the early-time effects, such as caging, do depend strongly on t_0 and indeed disappear if
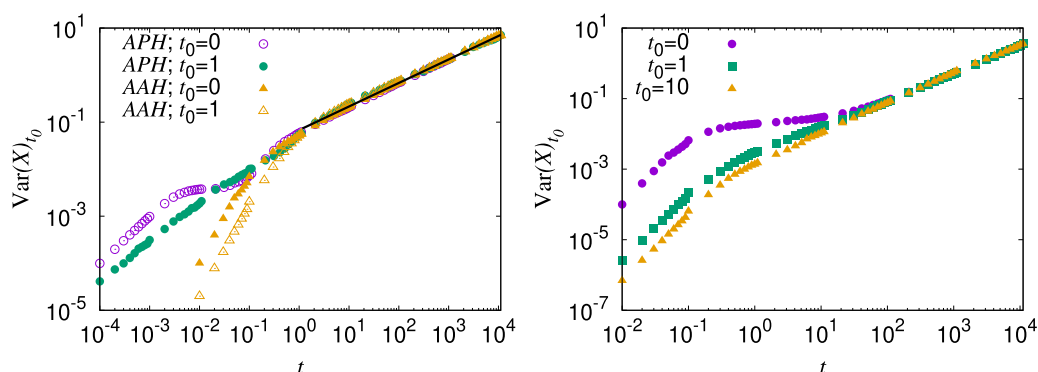
Figure C1. $\mathrm{Var}(X)$ against time for different system ages t_0 when observations begin at $t = 0$. (Left) APH and AAH results. $N = 2000, \rho = 10, v = 1 = \gamma, D = 0.5$. The black solid line is $\xi_{\mathrm{AAH}}\sqrt{t}$, with ξ_{AAH} obtained via fitting the AAH data for $t_0 = 0$. All data averaged over at least 10^4 realizations or more. (Right) The same for AAN with $N = 4000, \rho = 10$. For all AAH and AAN cases, $\Delta t = 0.01$. For APH data, $\Delta t = 0.0001$ for $t \leqslant 1$ and $\Delta t = 0.01$ for $t > 1$ (overlap of data sets checked in the range $1 \leqslant t \leqslant 10$).

t_0 is large enough. This simply means that the caging in these 1D systems is transient, and to capture it properly, observations need be taken preferably right from the start of the experiment. From figure C1 we can see that the tracers become more and more constricted as $t_0 \uparrow \infty$, which effectively means that the respective tracers remain stuck against their neighbours. Therefore this limit can be viewed as one in which caging remains present but the cage-size becomes zero.

References

[1] Harris T E 1965 *J. Appl. Probab.* **2** 323
[2] Richards P M 1977 *Phys. Rev.* B **16** 1393
[3] Alexander S and Pincus P 1978 *Phys. Rev.* B **18** 2011
[4] Krapivsky P L, Mallick K and Sadhu T 2014 *Phys. Rev. Lett.* **113** 078101
[5] Hegde C, Sabhapandit S and Dhar A 2014 *Phys. Rev. Lett.* **113** 120601
[6] Cividini J and Kundu A 2017 *J. Stat. Mech.* 083203
[7] Hodgkin A L and Keynes R D 1955 *J. Physiol.* **128** 61
[8] Wei Q-H, Bechinger C and Leiderer P 2000 *Science* **287** 625
[9] Li G-W, Berg O G and Elf J 2009 *Nat. Phys.* **5** 294
[10] Kaerger J and Ruthven D M 1992 *Diffusion in Zeolites and Other Microporous Solids* (New York: Wiley)
 Chen N Y, Degnan T F and Smith C M 1994 *Molecular Transport and Reaction in Zeolites* (New York: VCH)
[11] Arratia R 1983 *Ann. Probab.* **11** 362
[12] Cooper G M 2000 *The Cell: A Molecular Approach* (Sunderland (MA), MA: Sinauer Associates)
[13] Gupta S, Majumdar S N, Godrèche C and Barma M 2007 *Phys. Rev.* E **76** 021112
[14] Rajesh R and Majumdar S N 2001 *Phys. Rev.* E **64** 036103
[15] Berg H C 2004 *E. Coli in Motion* (Heidelberg: Springer)
[16] Tailleur J and Cates M E 2008 *Phys. Rev. Lett.* **100** 218103
[17] Weiss G H 2002 *Physica* A **311** 381
[18] Banerjee T, Majumdar S N, Rosso A and Schehr G 2020 *Phys. Rev.* E **101** 052101
[19] Dhar A *et al* 2019 *Phys. Rev.* E **99** 032132
[20] Cates M E and Tailleur J 2013 *Europhys. Lett.* **101** 20010
[21] Gradenigo G and Majumdar S N 2019 *J. Stat. Mech.* 053206
[22] Mori F, Le Doussal P, Majumdar S N and Schehr G 2021 *Phys. Rev.* E **103** 062134

[23] Ben Dor Y *et al* 2019 *Phys. Rev.* E **100** 052610
[24] Evans M R and Majumdar S N 2018 *J. Phys. A: Math. Theor.* **51** 475003
[25] Slowman A B, Evans M R and Blythe R A 2016 *Phys. Rev. Lett.* **116** 218101
[26] Keta Y-E *et al* 2021 *Phys. Rev.* E **103** 022603
[27] Le Doussal P, Majumdar S N and Schehr G 2019 *Phys. Rev.* E **100** 012113
[28] Le Doussal P, Majumdar S N and Schehr G 2021 arXiv:2105.11838
[29] Cates M E and Tailleur J 2015 *Annu. Rev. Condens. Matter Phys.* **6** 219
[30] Bechinger C *et al* 2016 *Rev. Mod. Phys.* **88** 045006
[31] Put S, Berx J and Vanderzande C 2019 *J. Stat. Mech.* 123205
[32] Singh P and Kundu A 2021 *J. Phys. A: Math. Theor.* **54** 305001
[33] Bertrand T, Illien P, Bénichou O and Voituriez R 2018 *New J. Phys.* **20** 113045
[34] Thompson A G, Tailleur J, Cates M E and Blythe R A 2011 *J. Stat. Mech.* P02029
[35] Soto R and Golestanian R 2014 *Phys. Rev.* E **89** 012706
[36] Shakerpoor A, Flenner E and Szamel G 2021 arXiv:2102.11240
[37] Fily Y, Kafri Y, Solon A P, Tailleur J and Turner A 2018 *J. Phys. A: Math. Theor.* **51** 044003
[38] Solon A P, Fily Y, Baskaran A, Cates M E, Kafri Y, Kardar M and Tailleur J 2015 *Nat. Phys.* **11** 673
[39] Sepúlveda N and Soto R 2016 *Phys. Rev.* E **94** 022603
[40] Dolai P, Das A, Kundu A, Dasgupta C, Dhar A and Kumar K V 2020 *Soft Matter* **16** 7077
[41] Dolai P, Simha A and Mishra S 2018 *Soft Matter* **14** 6137
[42] Wittkowski R, Stenhammar J and Cates M E 2017 *New J. Phys.* **19** 105003
[43] Banerjee T, Basu U and Maes C 2020 *Phys. Rev.* E **101** 062130
[44] Ben-Isaac E *et al* 2015 *Phys. Rev.* E **92** 012716
[45] Razin N, Voituriez R and Gov N S 2019 *Phys. Rev.* E **99** 022419
[46] Maes C 2020 *Phys. Rev. Lett.* **125** 208001
[47] Granek O, Kafri Y and Tailleur J 2021 arXiv:2108.11970
[48] Sadhu T and Derrida B 2015 *J. Stat. Mech.* P09008
[49] Krapivsky P L, Redner S and Ben-Naim E 2010 *A Kinetic View of Statistical Physics* (Cambridge: Cambridge University Press)
[50] Derrida B and Gerschenfeld A 2009 *J. Stat. Phys.* **137** 978
[51] Leibovich N and Barkai E 2013 *Phys. Rev.* E **88** 032107
[52] Rozenfeld R, Łuczka J and Talkner P 1998 *Phys. Lett.* A **249** 409
[53] Gudimchuk N B and McIntosh J R 2021 *Nat. Rev. Mol. Cell Biol.* **22** 777
[54] Percus J K 1974 *Phys. Rev.* A **9** 557
[55] Barkai E and Silbey R 2010 *Phys. Rev.* E **81** 041129
[56] Mallmin E, Blythe R A and Evans M R 2021 *J. Stat. Mech.* 013209
[57] Lobaskin I and Evans M R 2020 *J. Stat. Mech.* 053202
[58] Lee C F 2013 *New J. Phys.* **15** 055007
[59] Hafner A E, Santen L, Rieger H and Shaebani M R 2016 *Sci. Rep.* **6** 37162
[60] Bénichou O, Loverdo C, Moreau M and Voituriez R 2011 *Rev. Mod. Phys.* **83** 81
[61] Shröder T B and Dyre J C 2020 *J. Chem. Phys.* **152** 141101
[62] Kob W and Andersen H C 1995 *Phys. Rev.* E **51** 4626
[63] Berthier L, Flenner E and Szamel G 2019 *J. Chem. Phys.* **150** 200901
[64] Fodor É, Guo M, Gov N S, Visco P, Weitz D A and van Wijland F 2015 *Europhys. Lett.* **110** 48005
[65] Majumdar S N and Barma M 1991 *Phys. Rev.* B **44** 5306
[66] Cividini J, Kundu A, Majumdar S N and Mukamel D 2016 *J. Stat. Mech.* 053212
[67] Parry B R, Surovtsev I V, Cabeen M T, O'Hern C S, Dufresne E R and Jacobs-Wagner C 2014 *Cell* **156** 183
[68] Christensen S M, Munkres I and Vannette R L 2021 *Curr. Biol.* **31** 4373–80
[69] Manirajan B A *et al* 2019 *Old Herborn University Seminar Monograph 33: The Flowering of the Plant Microbiome and the Human Connection* ed P J Heidt, J Versalovic, M S Riddle, V Rusch (Herborn-Dill: Old Herborn Universiity Foundation) p 62 (http://old-herborn-university.de/)
[70] Zausch J, Horbach J, Laurati M, Egelhaaf S U, Brader J M, Voigtmann T and Fuchs M 2008 *J. Phys.: Condens. Matter.* **20** 404210
[71] Reichert J and Voigtmann T 2021 *Soft Matter* **17** 10492